Norges miljø- og
biovitenskapelige
universitet

Master's Thesis 2021 30 ECTS

Faculty of Environmental Sciences and
Natural Resource Management (MINA)

CFD Simulations of Local Wind Fields, a Parametric Study

Vincent Kortebein Birkeland
Renewable Energy

Acknowledgements

This master thesis marks the end of my two years master program Renewable Energy at the Norwegian University of Life Sciences.

This thesis is written in collaboration with WindSim AS, a wind simulation software provider. The assignment is given by Arne Reidar Gravdahl, CTO and founder of WindSim AS, and the results will hopefully be of value in terms of determining the parameters in wind simulation models.

I would like to give my greatest thanks to my supervisor (associate) Professor Arne Reidar Gravdahl for his support and for giving me access to WindSim resources and allowing me to participate in WindSim Basic Course. I would also like to thank Pablo Duran, Ph.D and (previous) Wind Consultant at WindSim for his technical support and guidance.

Zephyr AS is greatly acknowledged for their generosity in supplying me with measurement data.

A big thanks to my faculty at NMBU who gave me a 1-year permit during a difficult time for me and my family. Thanks to their understanding and facilitation I can complete this project. Thanks to my supervisor at NMBU, Professor Muyiwa Samuel Adaramola for his support and motivation.

Finally, I would like to thank my family for their support and encouragement through the last year.

Norwegian University of Life Sciences
Ås, December 15, 2021

Vincent Kortebein Birkeland

Abstract

Establishing the local wind fields using a simulation software is an important part of the wind resource assessment. In this study the WindSim software, utilizing the Computational Fluid Dynamics (CFD) method, is used to simulate the local wind fields in an area in Southwest Norway. A total of 20 digital terrain model grids are created. Every grid has different numerical settings, with respect to the horizontal- and vertical resolution, domain buffer size and refinement area size. By comparing the vertical profiles at 29 specific turbine positions, the same positions in all 20 cases, the sensitivity of the parameters can be analysed.

When performing CFD simulations of the wind fields the assumption is that a higher resolution model produces more accurate results. The main challenges of utilizing finer grids in CFD modelling today is the time consumption. The present exponential growth in computing power and the introduction of cloud computing will reduce these challenges greatly. The latter without investing in expensive local high-end computers.

The sensitivity study reveals significant differences in the results with respect to the set grid parameters. The most sensitive parameter is the horizontal resolution of the grid. Higher resolution grids typically increase the variability of the results, giving higher maximum values and lower minimum values.

Sammendrag

Etablering av de lokale vindfeltene ved hjelp av en simuleringsprogramvare er en viktig del av enhver vindressursvurdering. I denne studien brukes WindSim-programvaren, som benytter numerisk fluiddynamikk metoden, for å simulere de lokale vindfeltene i et område Sørvest i Norge. Det lages totalt 20 digitale terrengmodeller. Hver modell har forskjellige numeriske innstillinger, med hensyn til horisontal- og vertikal oppløsning, størrelse på domene buffer og avgrensningsområde. Ved å sammenligne vertikale profiler for 29 spesifikke turbinposisjoner, likt for alle 20 modeller, kan sensitiviteten til parameterne analyseres.

Ved simulering av vindfelt antas det at en modell med høyere oppløsning gir mer nøyaktige resultater. Hovedutfordringen ved å bruke høyere oppløsning i numerisk fluiddynamikk i dag, er tidsforbruket. Den eksponentielle veksten i datakraft og introduksjon av sky-løsninger vil redusere disse utfordringene betraktelig. Sistnevnte uten å investere i kostbare lokale avanserte datamaskiner.

Sensitivitetsstudien avdekker betydelige forskjeller i resultatene med hensyn til de ulike numeriske innstillingene. Den mest sensitive parameteren er den horisontale oppløsningen. Modeller med høyere oppløsning øker vanligvis variasjonen i resultatene, og gir høyere maksverdier og lavere minimumsverdier.

Contents

Acknowledgements 3
Abstract 5
Sammendrag 6
List of Figures 10
List of Tables 12
Abbreviations and Definitions 13
1.0 Introduction 14
1.1 Thesis Outline 15
2. Theoretical Background 16
2.1 Computational Fluid Dynamics 16
2.1.1 Navier-Stokes 16
2.1.2 Navier-Stokes and turbulence 17
2.1.3 Reynolds Averaged Navier Stokes Equations (RANS) 17
2.1.4 Turbulence Model 18
2.2 Initial Conditions and Boundary Conditions 18
2.3 Resolution & Grid 19
2.3.1 Grid File 19
2.3.2 Roughness 19
2.3.3 Refinement area and buffer zone 19
2.3.4 Vertical Distribution 19
2.3.5 Sectors 20
2.3.6 Grid independence 20
3. Methodology 21
3.1 Defining the Base Case 21
3.2 Numerical parameter matrix 22
3.3 Cases 23
3.3.1 Resolution 23
3.3.2 Domain buffer 24

3.3.3 Refinement area 25
3.3.4 Vertical Layers 26
3.4 Site Description 27
3.4.1 Terrain Model 27
3.5 WindSim Modules 29
3.5.1 Terrain Module 29
3.5.2 Wind Fields Module 31
3.5.2.1 Boundary and initial conditions 31
3.5.2.2 Physical models 31
3.5.2.3 Iterations and convergence criteria 31
3.5.3 Objects Module 32
3.5.3.1 Turbine Positions 32
3.5.3.2 Objects 33
3.5.4 Results Module 34
3.6 Data Filtering 35
3.6.1 Vertical Profiles 35
3.6.2 Normalizing the Wind Speed 36
4. Results 37
4.1 Resolution 37
4.2 Domain 39
4.3 Refinement Area 42
4.4 Vertical Distribution 43
4.5 Summary Presentations 45
5. Discussion 46
5.1 Resolution 46
5.2 Domain 49
5.3 Refinement area 50
5.4 Vertical Distribution 52
6. Conclusion 55

7. Future Improvements/Further Research..... 56

References..... 57

List of Figures

Figure 1 Horizontal grids for cases S6 (a), S5 (b), S4 (c), S3 (d), S1 (e) and S2 (f) 23
Figure 2 Horizontal grids for cases S7 (a), S8 (b), S9 (c), S1 (d), S10 (e), S11 (f) and S12 (g)..... 24
Figure 3 Horizontal grids for cases S13 (a), S14 (b), S1 (c), S15 (d), S16 (e) and S17 (f)..... 25
Figure 4 The vertical grid for cases S18 (a), S1 (b), S19 (c) and S20 (d). All grids have a geometric distribution 26
Figure 5 Overview of the Nevlandsheia area in Southwest Norway (a). Zoomed-in view of the area (b). The turbines are placed along the red line. The three met masts are located on the corners of the triangle (white dots), only the two met masts on the south corners will be used as reference..... 27
Figure 6 Examples of the extension of the domain, the DTM 10 with 11km extension for case S1 (a) and the DTM 25 with 31km extension for case S1 (b) and S10 (c). The legend shows the elevation.. 28
Figure 7 The Corine Land Cover roughness layer for the Nevlandsheia area, the red triangle roughly represents the turbine area (a). The roughness values for the terrain in the WindSim terrain-module (b) 28
Figure 8 Property settings for the Terrain module in the WindSim interface showing the two different settings for refinement type. Refinement area (a) and refinement/blocking file (b)..... 29
Figure 9 The geometrical distribution of the vertical layers grid (z) as shown in the report section of the Terrain module. Geometric Distribution (a) Arithmetic distribution (b) 30
Figure 10 Open area index for the west-east (a) and south-north (b) traverse for the base case 30
Figure 11 The properties settings for the Wind Fields module in the WindSim Software interface 31
Figure 12 The spot value for the residuals displayed in the report section of the Wind fields module in the WindSim interface 32
Figure 13 All turbines placed in the WindSim Objects module 3D viewer; the triangles are the turbines in the 3D viewer (a). Turbine positions and names (b). The legend shows the terrain elevation 33
Figure 14 Objects module properties settings..... 33
Figure 15 Exporting the vertical profiles after running the Objects module (a). Vertical profile .txt example (b) 34
Figure 16 The vertical profile for every turbine is imported to excel and interpolated to match the reference heights of the met masts..... 35
Figure 17 Normalized wind speed for all turbine positions in cases S2-S6. Displayed here for heights 19 (a), 49 (b) & 100m (c) above the terrain..... 38
Figure 18 The simulated wind speeds at 19 (a), 49 (b) & 100m (c) above ground for numerical setting S2 39
Figure 19 The simulated wind speeds at 19 (a), 49 (b) & 100m (c) above ground for numerical setting S6 39

Figure 20 Normalized wind speed for all turbine positions in cases S7-S12. Displayed here for heights 19 (a), 49 (b) & 100m (c) above the terrain. 40
Figure 21 The simulated wind speeds at 19 (a), 49 (b) & 100m (c) above ground for numerical setting S7 41
Figure 22 The simulated wind speeds at 19 (a), 49 (b) & 100m (c) above ground for numerical setting S12 41
Figure 23 Normalized wind speed for all turbine positions in cases S13-S17. Displayed here for heights 19 (a), 49 (b) & 100m (c) above the terrain 42
Figure 24 The simulated wind speeds at 19 (a), 49 (b) & 100m (c) above ground for numerical setting S13 43
Figure 25 The simulated wind speeds at 19 (a), 49 (b) & 100m (c) above ground for numerical setting S17 43
Figure 26 Normalized wind speed for all turbine positions in cases S18 - S20 at 19 (a), 49 (b) & 100m (c) above the terrain 44
Figure 27 The simulated wind speeds at 19 (a), 49 (b) & 100m (c) above ground for numerical setting S18 45
Figure 28 The simulated wind speeds at 19 (a), 49 (b) & 100m (c) above ground for numerical setting S20 45
Figure 29 Comparison of numerical setting S2 (a) and S6 (b) at height above terrain, H = 100. Green turbines represent higher simulated wind speed-ups for the S2 case. Yellow turbines represent higher simulated wind speed-ups for S2 at lower heights but equals out further above ground. White turbines have highest simulated wind speed-ups for the S6 case 47
Figure 30 Vector plots for wind speed from 0-1.2 m/s in cases S3 (a), S1 (b) & S2 (c) with a resolution of 50x50, 25x25 and 10x10 meters respectively. The vectors show that the wind is moving in multiple directions and the largest recirculation zone is clearly in the high-resolution model (c). Height above terrain, H = 19 47
Figure 31 Vector plots for wind speeds 0 - 1.2 m/s in cases S3 (a), S1 (b) & S2 (c) with a resolution of 50x50, 25x25 and 10x10 meters respectively. The recirculation zone is close to absent in S3 (a), but still very visible in S2 (c). Height above terrain, H = 49 48
Figure 32 Development of low wind speed zones at 100m above the terrain for models S5 (a), S4 (b), S3 (c) & S1 (d) 48
Figure 33 The simulated horizontal wind speed for S9 (a), S1 (b) & S10 (c). The marked area is highlighting the ridge/hill upstream the wind farm. The white arrow resembles the inlet wind direction. Height above terrain, H =100 49
Figure 34 2D wind speed graphics for the S1 (a) and S16 (b) with the grid displayed. The green turbines are T25, T2 and T24 (North to South). Scalar value is the simulated wind speed at the height above terrain H = 100 51

Figure 35 2D wind speed graphics incl. horizontal grid for S1(a), S16(b) and S17(c). Green turbines T25, T2 and T24 (North to South). Black outlined turbines T3 (Top) and T23 (Bottom). Scalar value is the simulated wind speed at the height above terrain H=100 52
Figure 36 Vertical plot of the simulated wind speed at respective heights at turbine position M1 53
Figure 37 Vertical plot of the simulated wind speed at respective heights at turbine position T23 53
Figure 38 The distribution of the first 20 layers in the vertical for cases S18 (a), S1 (b), S19 (c) and S20 (d) 54

List of Tables

Table 1 Standard values for the k-e model constants 18
Table 2 The numerical settings for all cases 22

Abbreviations and Definitions

CFD	Computational Fluid Dynamics
CLC	Corine Land Cover
DTM	Digital Terrain Model
GIS	Geographic Information System
GM	Global Mapper
M	Met mast
RANS	Reynolds Averaged Navier-Stokes
T	Turbine
WAsP	Wind Atlas Analysis and Application Program
WRA	Wind Resource Assessment

Reynolds number	A dimensionless number used in fluid mechanics to indicate whether a fluid flow past a body or in a duct is steady or turbulent
Eddies	A circular movement of water, air or smoke.
Eddy viscosity	The proportionality factor describing the turbulent transfer of energy as a result of moving eddies, giving rise to tangential stresses

1.0 Introduction

Computational Fluid Dynamics (CFD) is a widely used method to do Wind Resource Assessment (WRA) and wind farm modelling in recent years. A variety of methods exist for the purpose of simulating wind fields, which compared to field measurements, offer three-dimensional wind fields of high resolution. Linear models such as Wind Atlas Analysis and Application Program (WAsP) were originally used to calculate the wind fields due to their simpler approach with higher efficiency and satisfying accuracy in terrain with moderate slopes (Palma et al., 2008). In more complex terrain CFD has become both practical and necessary as the computational capacity has increased drastically combined with the need for more accurate wind field predictions. The majority of CFD simulation software solves the Reynold-Average Navier-Stokes (RANS) equations. The RANS equations are time independent and provide the steady state wind velocity at each grid point (Dhunny, Lollchund and Rughooputh, 2017).

WindSim, a state-of-the-art CFD wind simulation software has been used and evaluated on several occasions in industrial settings and academia. The results of WindSim compared to other methods in complex terrain has been done by multiple groups with better performance in the WindSim CFD-model ((Palma et al., 2008), (Llombart et al., 2006), (Wallbank, 2008), (Dhunny, Lollchund and Rughooputh, 2016), (Ramos et al., 2017)). Cattin, Schaffner and Kunz (2006) validated WindSim to fulfil the requirements for wind modelling in highly complex terrain at 7 Alpine sites. When simulating wind fields over a complex terrain the creation of a high-quality 3D terrain model is crucial. The shape and detail of this terrain model is essential to obtaining the quality results necessary to realise a profitable wind farm project. How are the parameter values determined and how does a change in the numerical parameters affect the simulated results?

The main objective of this study is mapping the sensitivity of a selection of simulation parameters used in the WindSim software when calculating the wind fields in complex terrain. Domain buffer size, refinement area size, horizontal- and vertical resolution are investigated to find the sensitivity of each variable. The preferred outcome is to find parameter values where independency is obtained, meaning an increase or decrease in the value of a variable will no longer affect the results. All simulations will be performed on a digital terrain model of the Nevlandsheia area in Southwest Norway, and the simulation results will be validated by comparing it to measurement data for the relevant site.

1.1 Thesis Outline

The thesis outline is as follows. Chapter 2 presents the relevant theoretical background for wind simulation using the CFD method in WindSim. Chapter 3 shows the numerical settings used to create the terrain model grids, the settings and monitoring of the wind field simulations and the data filtering. Chapter 4 presents the results of the wind field simulations before the results are discussed and concluded in chapters 5 and 6.

2. Theoretical Background

To understand the impact of the different parameters in the simulated model, a basic understanding of the theoretical background is necessary. This chapter will give a basic explanation of the relevant physical theories and parameters associated with wind turbines and CFD-modelling.

2.1 Computational Fluid Dynamics

CFD is the analysis and numerical problem solving of a system containing fluid flow, gas, and liquids, by means of computer-based simulation. The method is powerful and used within numerous fields and industries, such as hydrology, meteorology, and aerodynamics. Three physical laws serve as the foundation for all CFD models, and they are stated as follows:

(1) The mass of fluid is conserved.

(2) Newton's second law: The rate of change of momentum equals the sum of forces on a fluid particle.

(3) First law of thermodynamics: The rate of change of energy is equal to the sum of the rate of heat addition to and the rate of work done on a fluid particle (Versteeg and Malalasekera, 2007**).**

The fundamental principles above can be expressed as mathematical equations. For a fluid flow in the form of unsteady Navier-Stokes equations. The CFD determines a numerical solution to the mathematical equations while taking the solution through time and space to gain a numerical representation of the complete flow field of interest. To be able to compute a numerical solution, the case is discretized: Space is split into a number of cells for which the flow is solved. Within WRA the time dependency can be excluded, and a steady state wind field is established for certain boundary conditions.

Contrary to diagnostic models, which calculates the statistics of the wind by parameterizing the impact of obstacles, roughness, and topography, CFD modelling calculates the three-dimensional flow field of the wind. In many ways like a virtual wind tunnel (Cattin, Schaffner and Kunz, 2006**).**

2.1.1 Navier-Stokes

The Navier-Stokes equations describe the motion of fluids and are an application of Newton's second law, F=ma. The equations are non-linear, partial differential equations and do not establish an explicit relationship between the variables of interest. Instead, they establish associations of rates of change which link the variables. A solution of the Navier-Stokes equations is called a velocity field and describes the velocity of the fluid at a point in time.

2.1.2 Navier-Stokes and turbulence

The Navier-Stokes equations numerical solution for turbulent flow faces several challenges, primarily the extremely fine mesh required to capture the full range of length scales, but also the time consumption and the impractically large computational power requirement. As a result, turbulence is frequently handled in a "statistical" rather than an explicit manner, and methods like the *k-e* model (2.1.4 Turbulence Model) are used to model turbulent flow in practical CFD applications.

2.1.3 Reynolds Averaged Navier Stokes Equations (RANS)

The RANS equations are "*time-averaged*" Navier-Stokes equations and primarily used when modelling turbulent flow. The Reynolds decomposition is applied to the Navier-Stokes equations and defines the possibility of separating a flow variable into the mean component (time averaged) and the fluctuating component.

$$u(x,t) = \bar{u}(x) + u'(x,t) \qquad (1)$$

Where x = (x, y, z) is the positional vector, ū the time averaged component and u', the fluctuating component.

To model the flow field, WindSim utilises the RANS equations. Rather than using a time step approach to solve the flow calculations, this solution starts with the user's initial boundary conditions and works its way to a steady state solution (which reflects a time averaged solution). For the entire domain, this solution has one wind and one turbulence distribution (Berge et al., 2006).
The Navier-Stokes equations in Cartesian form:

$$\frac{\partial Ui}{\partial x_i} = 0 \qquad (2)$$

$$U_j \frac{\partial U_i}{\partial x_j} = -\frac{1}{\rho}\frac{\partial P}{\partial x_i} + \frac{\partial}{\partial x_j}\left(v\left(\frac{\partial U_i}{\partial x_j} + \frac{\partial U_j}{\partial x_i}\right) - \left(\overline{u_i u_j}\right)\right) \qquad (3)$$

U is the velocity, x is the positional component, P is the pressure, ρ is the density, v is the kinematic viscosity and the subscripts *i* and *j* defining unit vectors. With turbulence closure obtained by relating the Reynolds stresses to the mean velocity through turbulent viscosity.

$$\overline{u_i u_J} = -v_T\left(\frac{\partial U_i}{\partial x_j} + \frac{\partial U_j}{\partial x_i}\right) + \frac{2}{3}\delta_{ij}k \qquad (4)$$

Where v_T is the turbulent viscosity and *k* is the turbulent kinetic energy.

2.1.4 Turbulence Model

From a computational point of view the isotropic two equation models are viewed as lucrative out of the various turbulence models available for turbulence closure. The models are computationally less expensive and reasonably accurate. In this study the k-e model is chosen as the turbulence model. WindSim solves the equations for turbulent kinetic energy (k) and turbulent dissipation rate (e) to simulate the flow dynamics in complex terrain (Rameche Candane and Gravdahl, 2012).

The standard k-e model belongs to the family of eddy viscosity. Eddy viscosity, v_T, is calculated by an analytical equation. For high turbulent Reynolds numbers, the standard form of the k-e model may be summarised as:

$$v_T = C_\mu \frac{k^2}{\varepsilon} \quad (5)$$

$$\frac{\partial}{\partial x_i}(U_i\, k) = \frac{\partial}{\partial x_i}\left(\frac{v_T}{\sigma_k}\frac{\partial k}{\partial x_i}\right) + P_K - \varepsilon \quad (6)$$

$$\frac{\partial}{\partial x_i}(U_i\, \varepsilon) = \frac{\partial}{\partial x_i}\left(\frac{v_T}{\sigma_\varepsilon}\frac{\partial \varepsilon}{\partial x_i}\right) + C_{\varepsilon 1}\frac{\varepsilon}{k}P_K - C_{\varepsilon 2}\frac{\varepsilon^2}{k} \quad (7)$$

Here k is the turbulent kinetic energy, ε is the dissipation rate, v_T is the turbulent kinematic viscosity. The subscripts i and j are defining unit vectors. C_μ, σ_k, σ_ε, $C_{\varepsilon 1}$, $C_{\varepsilon 2}$ are the model constants and the standard values are displayed in the Table 1 below. P_K is the turbulent kinetic energy productions term:

$$P_K = v_T\left(\frac{\partial U_i}{\partial x_j} + \frac{\partial U_j}{\partial x_i}\right)\frac{\partial U_i}{\partial x_j} \quad (8)$$

Table 1 Standard values for the k-e model constants

C_μ	σ_k	σ_ε	$C_{\varepsilon 1}$	$C_{\varepsilon 2}$
0.09	1.0	1.3	1.44	1.92

2.2 Initial Conditions and Boundary Conditions

The overall time it takes for a numerical solution to reach convergence is solely determined by the original assumption. Patching the entire computational domain to values that are closer to the expected result is standard procedure. The computational domains examined in atmospheric flows are extremely large and so the computing time associated with such tasks is considerable. It is normal procedure, to accelerate the convergence, to begin with an initial profile for velocity and other turbulence variables such as the turbulent kinetic energy and the turbulent dissipation rate in order to accelerate convergence.

Information about the flow field must be supplied along the borders of the model. These boundary conditions are specified as analytical profiles or nesting. If the atmosphere is neutral the wind profiles are log profiles. Utilizing the log profile along the border is comparable to placing an infinite flat terrain upstream the 3D model. This assumption might be bad and so the results close to the borders should be handled with caution.

2.3 Resolution & Grid

The number of cells in the model and its extension determines the resolution. The model domain is gridded into cells to make up the nodes of which the calculations are performed. The higher the number of cells in the model, the higher the resolution. CFD- simulations can be very time consuming and therefore it is important to take simulation time into consideration. Using a higher resolution model, the simulation time needed is exponentially proportional to the number of cells.

2.3.1 Grid File

The grid file with extension .gws contains geospatial data and is used for organizing geospatial data such as maps, images, and GIS* databases. The grid file contains coordinates that can refer to any global orthogonal system.

2.3.2 Roughness

Roughness puts a value on the roughness heights of the terrain. By default, the variable roughness heights in WindSim are read from the .gws file, but alternatively a constant roughness height can be implemented in the model by specifying a non-zero value for the roughness height.

2.3.3 Refinement area and buffer zone

The model is divided into two main sections, a refinement area in the centre and a surrounding buffer zone. The refinement area is where the turbines will be installed, and as much and as thorough data as possible is wanted. The buffer zone is the outer section and represents the distance between the turbine area and the boundary.

2.3.4 Vertical Distribution

The vertical distribution includes the vertical layers of the computer model. In WindSim 60 vertical layers are allowed, they are distributed arithmetically from the terrain surface to the top-boundary of the model. In wind energy the areas closer to the terrain is of more importance as this is where the turbines are placed. To get a higher resolution in this area the vertical distribution can be altered.

Geometric and arithmetic distribution are two possible approaches where the vertical layers are no longer evenly distributed but concentrated in the lower levels of the vertical area.

2.3.5 Sectors

In CFD simulations the wind directions are divided into *n* - number of sectors. In the WindSim CFD-software the wind field calculations are done for several sectors. The standard is 12 sectors, but the flow calculations can also be performed with 24 or 36 sectors. If not limited by the set number of iterations the flow calculations run through every sector until a steady-state solution is found. The number of iterations can be increased and customized to fit the complexity and number of cells in the model to reach a steady-state solution. In a case with laminar flow, it can be assumed that the flow fields for a given sector is proportional to the incoming wind speed and their characteristics will not change with different wind speeds (Cattin, Schaffner and Kunz, 2006).

2.3.6 Grid independence

Grid independence is a term used to describe a model configuration in which adding more cells to the grid, making each volume cell smaller, has no significant impact on the results. The available computational resources determine the ability to create a grid independent solution as the size of the grid is limited by the memory allocation on the simulating computer. Wind field simulations over complex terrain where turbulence is high rarely achieves grid independence. The goal is to measure the error in the solutions by systematically increase the number of cells and comparing the wind profiles. If the error is reduced to a zero change in the solution for an increase, the solution is grid independent (**AIAA, 1998**).

3. Methodology

This chapter will present the planning and execution process of this parametric study. Defining a base case with inclusion of relevant numeric parameters. Generation of proper 3D terrain models, several time- and computational demanding wind field simulations and the placement of wind turbines to collect the wind profiles. Post simulation data processing with exports to excel and normalizing and interpolating vertical profiles for 29 wind turbines in 20 different cases. Compress all gathered data to be presented in an understandable way in the *Results* chapter.

3.1 Defining the Base Case

Defining the base case is related to the numerical settings used in commercial wind simulation today. The numerical settings are essential regarding simulation results, -time and hardware requirements. The base case represents standard parameter values and will be included as a comparison in all the displayed results. The time variable has not been accounted for because the cases of this study has been run on different computers. This is not seen as a major issue due to the rapid increase in computing capacity and introduction of cloud computing making the measured simulation times on a private computer irrelevant to commercial actors. The number of cells is specified in the numerical setting matrix and assumed increase of accuracy is related to the increase of total cells. Based on the results an increase in model size could be justified by an increase in the accuracy of the simulation. If the numerical results are not changing when further increasing the model size/number of cells, grid independence is achieved.

3.2 Numerical parameter matrix

The matrix (Table 2) presents the numerical settings for all cases. The *Domain Size* is km in X- and Y- direction. The *Grid Extension z (m)* is how high the grid extends above the point in the terrain with the highest elevation. The grid cells are the number of cells in X-, Y- and Z- direction. The resolution defines the smallest cell size possible in the model. The cell size is variable due to the predetermined refinement area in the model.

Table 2 The numerical settings for all cases

	Numerical Settings:	**Domain Size (km)**	**Grid Cells**	**Cells**	**Resolution (m)**	**Grid extention Z (m)**
	Case:	(Lx, Ly)	(nx, ny, nz)	(nx*ny*nz)	(dx, dy)	Lz
S1	Base_Case	24.1, 33.2,	242, 606, 24	3 519 648	25x25	3 643
S2	Reso 10	24.1, 33.2	534, 1444, 24	18 506 304	10x10	3 635
S3	Reso 50	24.1, 33.2	136, 318, 24	1 037 952	50x50	3 653
S4	Reso 100	24.1, 33.2	79, 170, 24	322 320	100x100	3 666
S5	Reso 200	24.1, 33.2	46, 92, 24	101 568	200x200	3 648
S6	Reso 500	24.1, 33.2	22, 40, 24	21 120	500x500	3 669
S7	Domain 1	6.1, 15.2	186, 550, 23	2 352 900	25x25	2 786
S8	Domain 3	10.1, 19.2	204, 568, 23	2 665 056	25x25	2 812
S9	Domain 5	14.1, 23.2	218, 582, 22	2 791 272	25x25	2 135
S10	Domain 20	44.1, 53.2	274, 638, 25	4 370 300	25x25	4 703
S11	Domain 25	54.1, 63.2	288, 652, 26	4 882 176	25x25	6 139
S12	Domain 30	64.1, 73.2	300, 664, 26	5 179 200	25x25	6 146
S13	Refine 0	22.1, 31.2	162, 526, 24	2 045 088	25x25	3 646
S14	Refine 0.5	23.1, 32.2	202, 566, 24	2 743 968	25x25	3 648
S15	Refine 3	28.1, 37.2	402, 766, 25	7 698 300	25x25	4 724
S16	Refine 5	32.1, 41.2	562, 926, 25	13 010 300	25x25	4 726
S17	Refine 7	36.1, 45.2	722, 1086, 25	19 602 300	25x25	4 707
S18	Vertical 10	24.1, 33.2	242, 606, 10	1 466 520	25x25	3 631
S19	Vertical 35	24.1, 33.2	242, 606, 35	5 132 820	25x25	3 664
S20	Vertical 50	24.1, 33.2	242, 606, 50	7 332 600	25x25	3 491

3.3 Cases

Table 2 presents the numerical settings for all cases in this study. To display the differences between the cases all the numerical grids will be presented below.

3.3.1 Resolution

There are a total of 6 cases with different horizontal resolution including the base case, respectively *S1*, *S2*, *S3*, *S4*, *S5* and *S6*. The finest mesh in the study is the *S2* with a horizontal resolution of 10x10m. The coarsest mesh in the study is the *S6* with a resolution of 500x500m. All horizontal grids for the resolution cases are displayed in Figure 1.

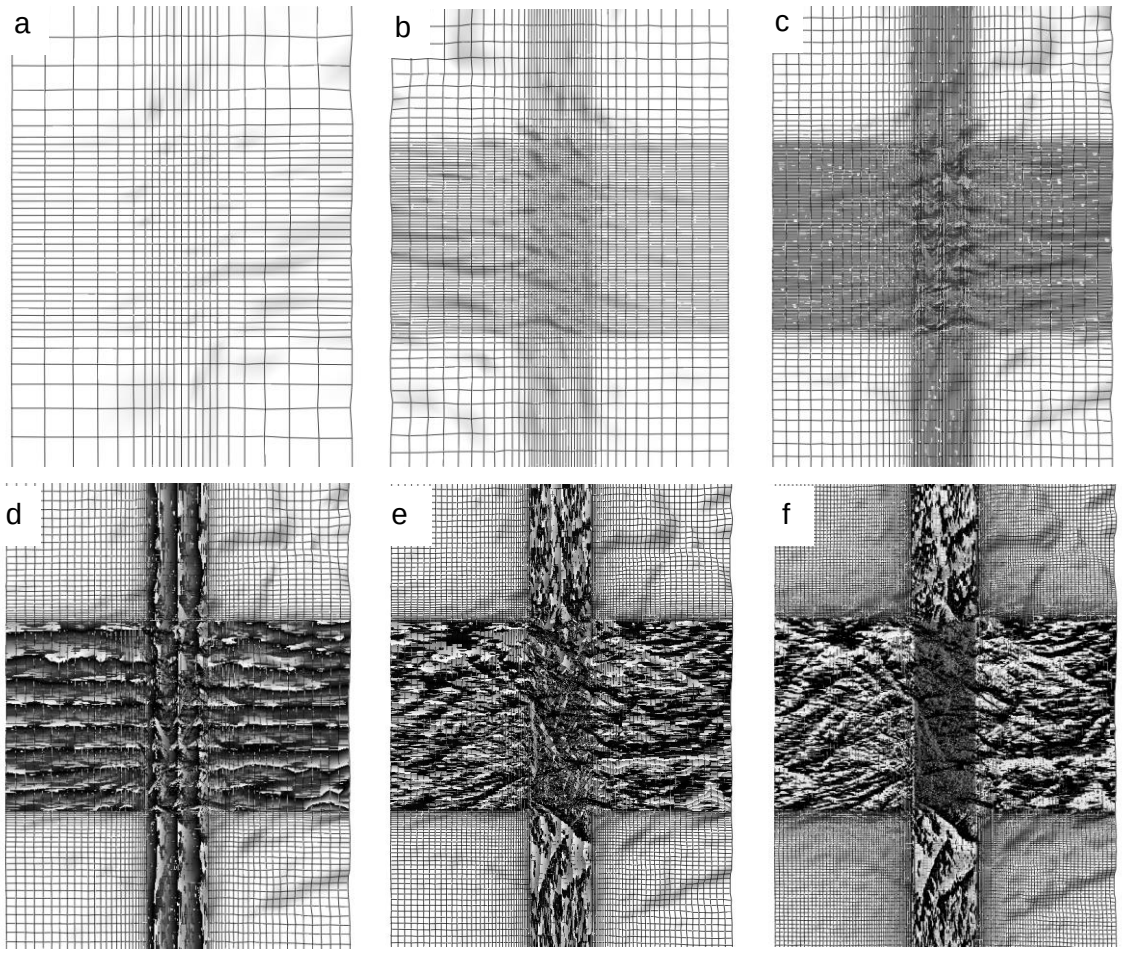

Figure 1 Horizontal grids for cases S6 (a), S5 (b), S4 (c), S3 (d), S1 (e) and S2 (f)

3.3.2 Domain buffer

The domain buffer parameter is represented in 7 different sizes, respectively: *S1*, *S7*, *S8*, *S9*, *S10*, *S11* and *S12*. The largest domain is found in the *S12* with a 30 km buffer, while the smallest is the *S7* with a 1 km buffer. All horizontal grids for the domain buffer cases are displayed in Figure 2.

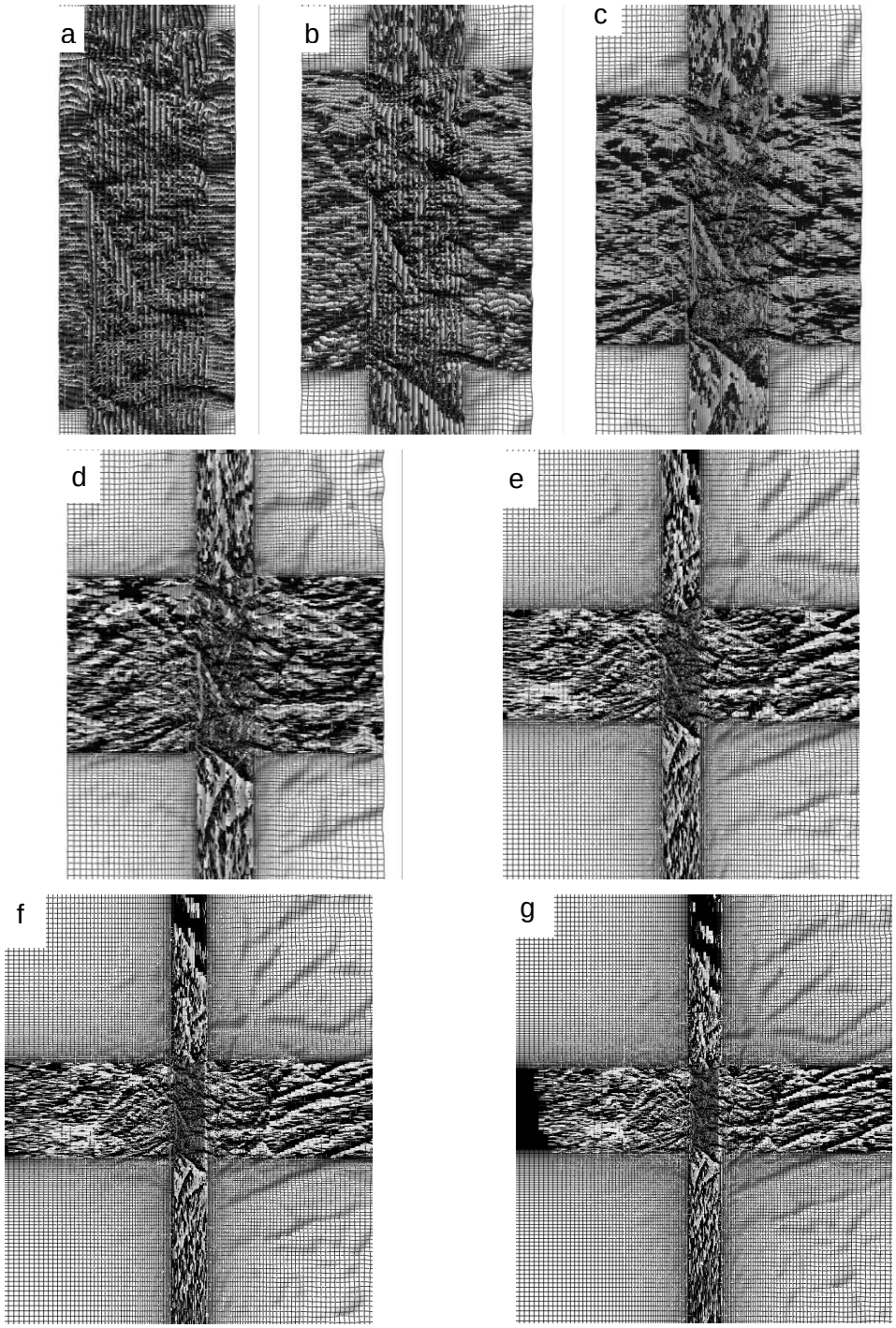

Figure 2 Horizontal grids for cases S7 (a), S8 (b), S9 (c), S1 (d), S10 (e), S11 (f) and S12 (g)

3.3.3 Refinement area

There are 6 variations of the refinement area setting, which is found in the *S1, S13, S14, S15, S16* and *S17* cases. The largest refinement area is represented by the *S17* case with 7km, while the smallest refinement area is 0km for *S13*. All the horizontal grids for the refinement area cases are displayed in Figure 3.

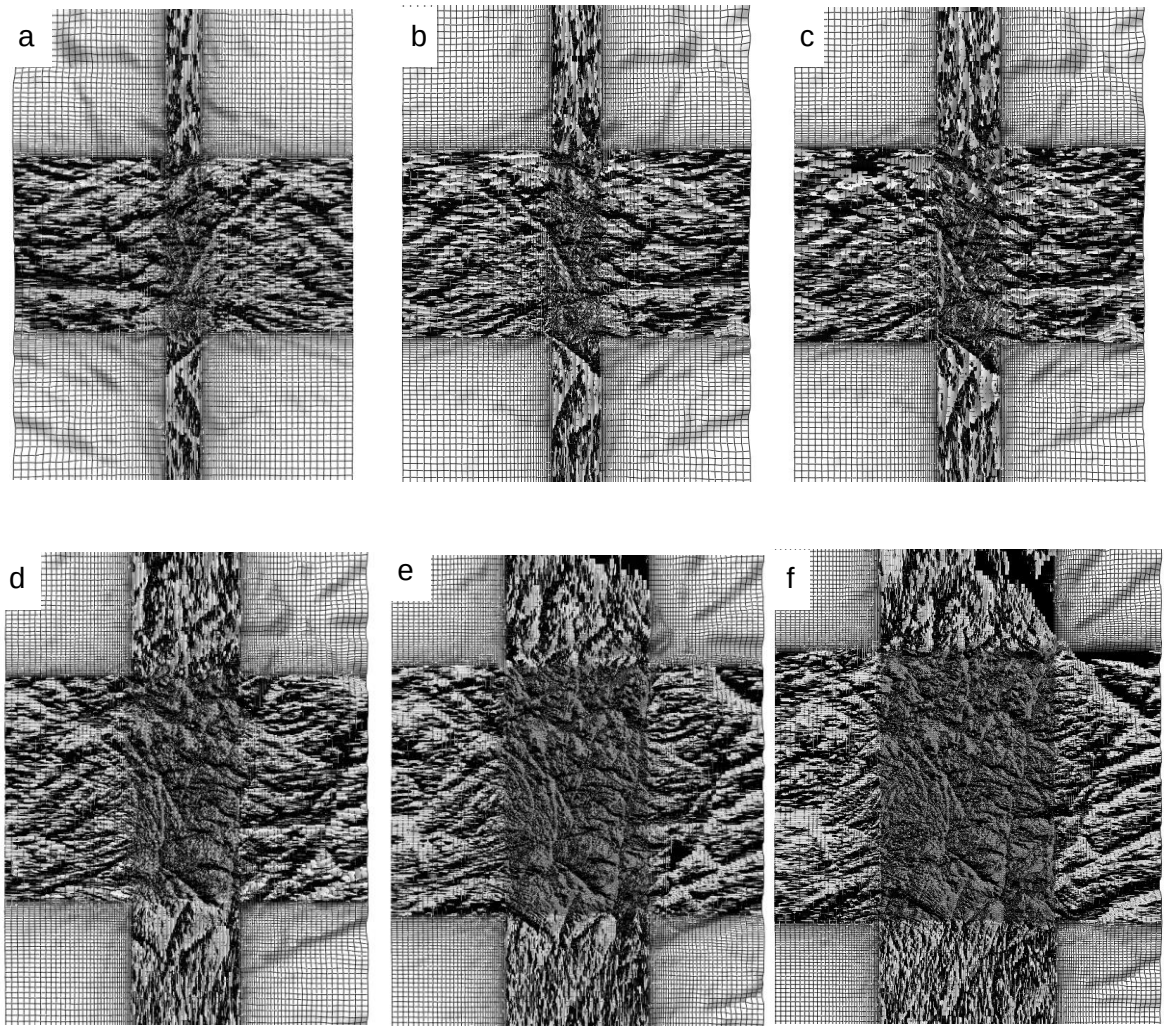

Figure 3 Horizontal grids for cases S13 (a), S14 (b), S1 (c), S15 (d), S16 (e) and S17 (f)

3.3.4 Vertical Layers

The last setting in the matrix is the number of vertical layers. The four cases with variable number of vertical layers are the *S1, S18, S19* and *S20.* The *S18* case has the lowest number of layers and a total of 10 layers in the vertical. The highest number of vertical layers is found in the *S20* case with a total of 50 layers. All cases have a geometrically distributed vertical grid and are displayed in Figure 4.

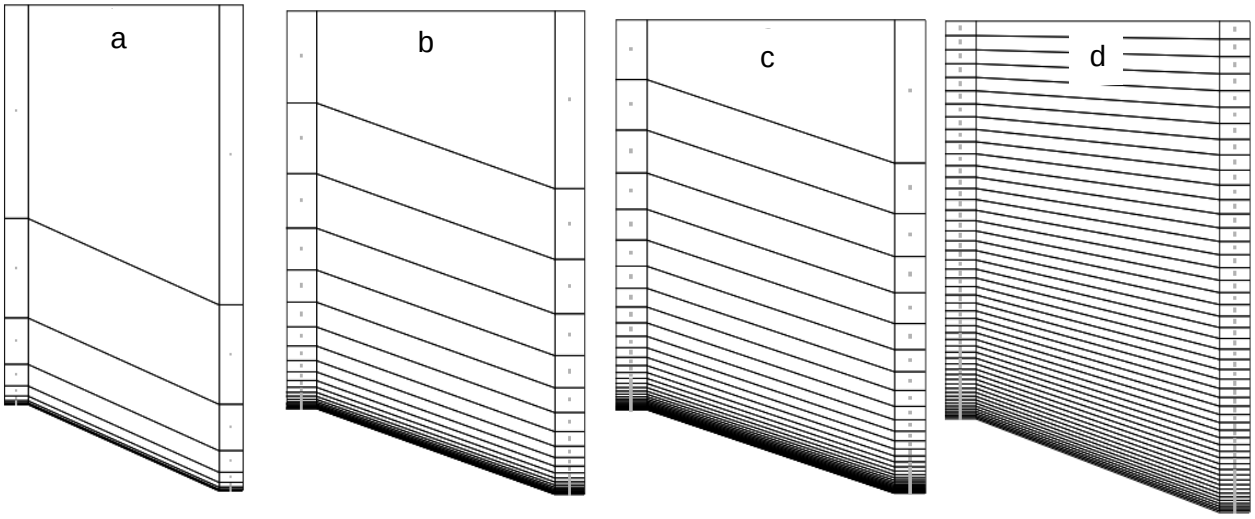

Figure 4 The vertical grid for cases S18 (a), S1 (b), S19 (c) and S20 (d). All grids have a geometric distribution

3.4 Site Description

The Nevlandsheia-Holmafjellet area in Southwest Norway (Figure 5) is selected as the case study. The area is located on a plateau with complex terrain at about 100-400 m.a.sl.

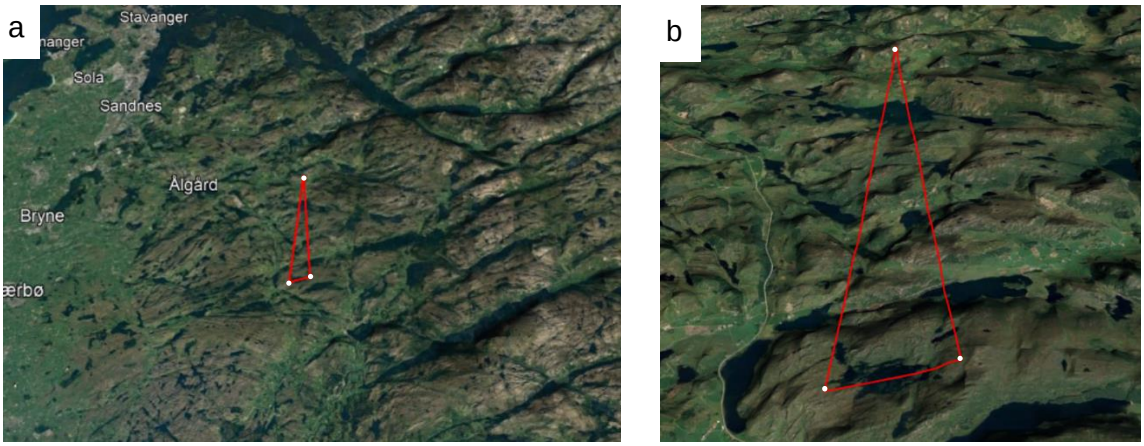

Figure 5 Overview of the Nevlandsheia area in Southwest Norway (a). Zoomed-in view of the area (b). The turbines are placed along the red line. The three met masts are located on the corners of the triangle (white dots), only the two met masts on the south corners will be used as reference

Data from three met masts in the area is used to validate the results of this parametric study. The met masts are set to be the centre of the simulation domain. Only the two southern met masts, Holmafjellet and Holmavatnet, will be used as validation points.

3.4.1 Terrain Model

To perform the wind simulations for the given site a 3D computer model of the terrain is required. The terrain data is downloaded as a Digital Terrain Model file (DTM) from Hoydedata (Hoydedata.no, n.d.), respectively DTM 10 and DTM 25 for the given case. The DTM 10 is needed for the highest resolution case model *S2*, while DTM 25 is sufficient for the other 19- cases. The files are respectively DTM 10 with a 11km buffer and DTM 25 with a 31km buffer as this reflects the maximum size of the simulation domain for the relevant cases (Figure 6).

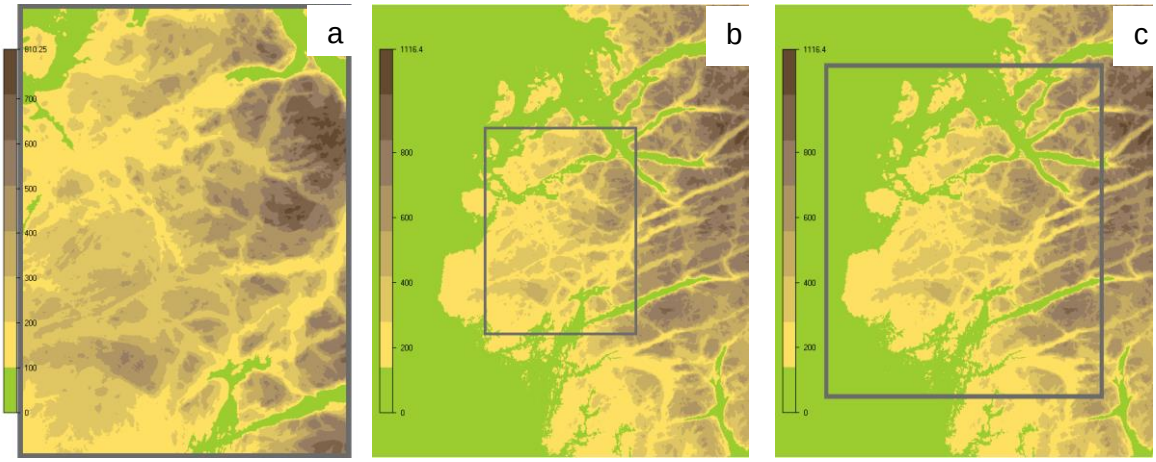

Figure 6 Examples of the extension of the domain, the DTM 10 with 11km extension for case S1 (a) and the DTM 25 with 31km extension for case S1 (b) and S10 (c). The legend shows the elevation

To create the 3D terrain model in WindSim a 2D dataset .gws file for the terrain model containing elevation and roughness data is required. To create the .gws file the Global Mapper (GM) software is used (Blue Marble Geographics, n.d.). In addition to the mentioned DTM-files a Terrain Roughness file is needed. The CORINE Land Cover Project V2018 (CLC) roughness map is used for this purpose and is merged with the DTM-files in GM (Copernicus.eu., 2018). The CLC contains the land cover data and assign a roughness value to the different land covers (Figure 7).

The WindSim grid file extension is integrated as an export option in GM. It is desired to export a file that covers the relevant area. To achieve this the relevant coordinates is plotted into the export properties. This procedure is done twice, once for the 31km DTM 25 and once for the 11km DTM 10.

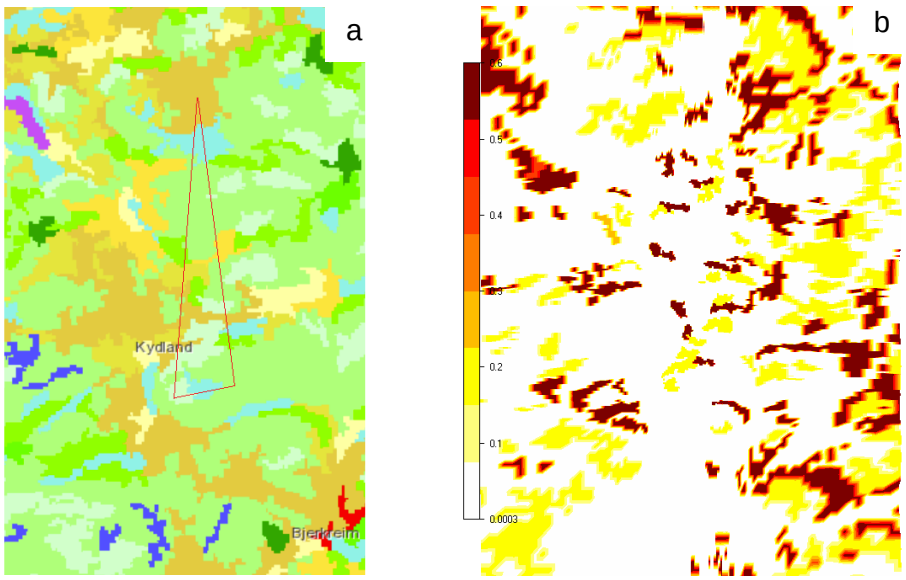

Figure 7 The Corine Land Cover roughness layer for the Nevlandsheia area, the red triangle roughly represents the turbine area (a). The roughness values for the terrain in the WindSim terrain-module (b)

3.5 WindSim Modules

The WindSim software has 6 modules: *Terrain, Wind Fields, Objects, Results, Wind Resources* and *Energy*. *Terrain, Wind Fields,* and *Objects* must be run in sequence and are interdependent, while the three last modules are different displays of the results and can be run independently. In this study the relevant modules are the three first modules which are required to obtain the desired results. In addition, the *Results* module will be used to present graphics and visual displays of points of interest. *Wind Resources* and *Energy* are irrelevant to the scope of this study.

3.5.1 Terrain Module

In the WindSim software the *Terrain* module is the first step in the WRA. The .gws file exported from GM is imported and the relevant setting for every case is done in the "*Properties menu*" (Figure 8). The DTM 25 file which is applied to every case except the *S2* (DTM 10) has a buffer of 31km from the turbine area. The relevance of this extension is limited to the case *S12* with the greatest domain size, thus the X- and Y-range in the "*Terrain Extension*" needs to be changed for all other cases. This is done by plotting the coordinates for the X- and Y-range for every case into the property settings in WindSim. The same procedure applies to the X- and Y-range for the refinement area.

a

1: Terrain extension	
Coordinate system	Global
X-range	**-31800; -7700**
Y-range	**6527500; 6560700**
Projection	**_UTM _WGS_84 33**
2: Roughness	
Roughness height	Read from grid.gws
3: Numerical model	
Automatic gridding	False
Refinement type	**Refinement area**
Refinement area, X-range	**-23767; -15733**
Refinement area, Y-range	**6538566; 6549634**
Height above terrain	Automatic
Horizontal griding	**Horizontal resolution**
Horizontal resolution	**25**

b

1: Terrain extension	
Coordinate system	Global
X-range	**-31800; -7700**
Y-range	**6527500; 6560700**
Projection	**_UTM _WGS_84 33**
2: Roughness	
Roughness height	Read from grid.gws
3: Numerical model	
Automatic gridding	False
Refinement type	**Use refinement file**
Refinement/blocking file	**simple_refinement_a.bws**
Orthogonalize 3-D grid	False
4: Smoothing	
Smoothing type	No smoothing
5: Forest	
Forest	Disregard forest

Figure 8 Property settings for the Terrain module in the WindSim interface showing the two different settings for refinement type. Refinement area (a) and refinement/blocking file (b)

The *Terrain* module is started when the terrain extension and refinement area extension is set. In this initial model generation, the vertical levels are distributed arithmetically with a factor of 0.1, which means the bottom layer is $1/10^{th}$ the size of the top layer. As wind turbines are placed on the ground with a typical hub height of 70-90 m the levels of interest in the vertical are closer to the ground. From the first terrain simulation the grid extension above the point in the terrain with the highest elevation is acquired. This height is used as input to create a geometric vertical distribution which is written into the WindSim project blocking file and saved as "*simple_refinement_a.bws*" (Figure 8). This new *.bws* file contains all information from the original file in addition to the updated values for the vertical distribution. The *Terrain* module is then run again with the updated blocking file. The

cells of the 3D terrain model are now more concentrated in the area where wind turbines operate, closer to the ground (Figure 9).

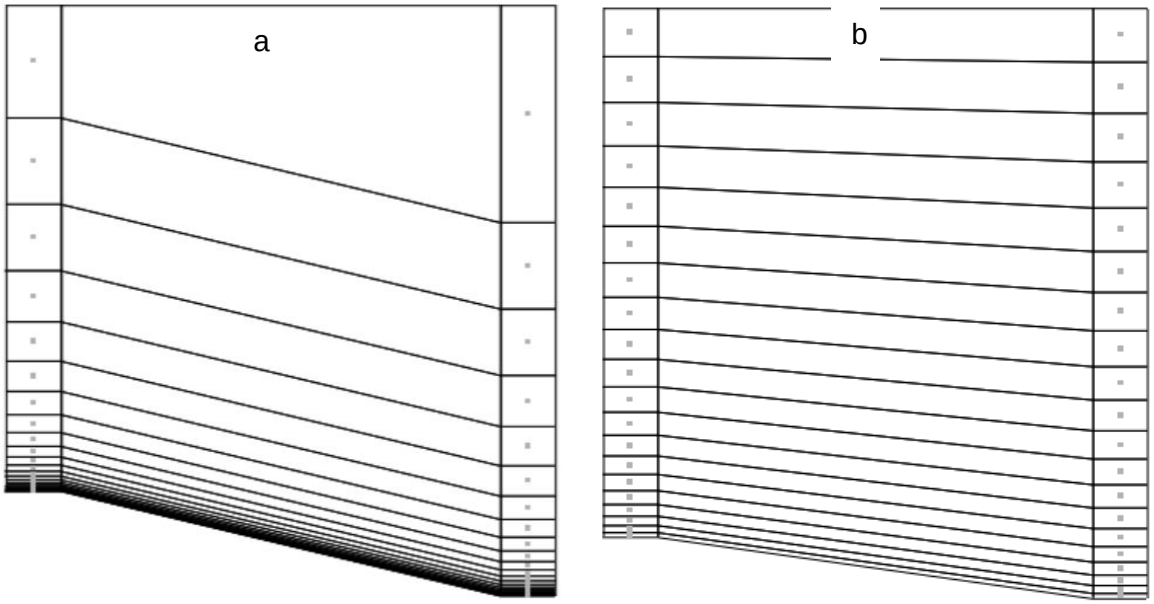

Figure 9 The geometrical distribution of the vertical layers grid (z) as shown in the report section of the Terrain module. Geometric Distribution (a) Arithmetic distribution (b)

The terrain grid file can be inspected in the *report* section of the *Terrain* module in the WindSim software.

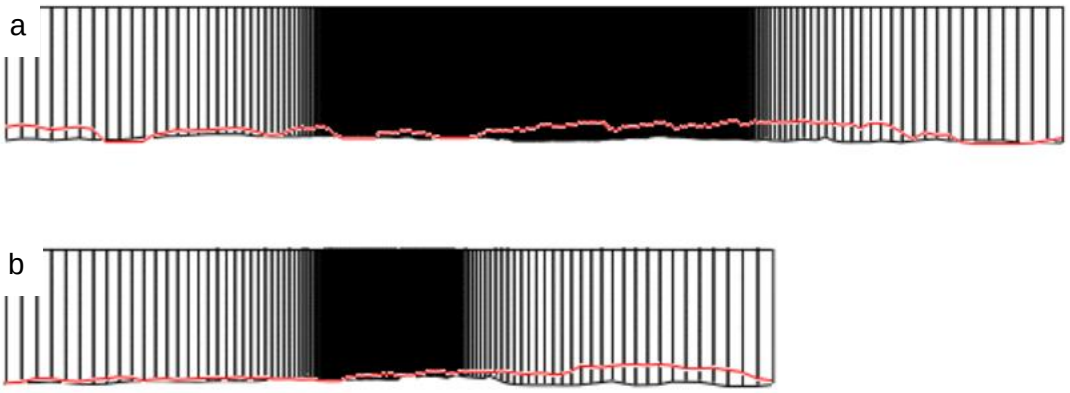

	Min (m^2)	Max (m^2)	Min/Max
Open area, west-east traverse	110446376	114588552	0.9639
Open area, south-north traverse	78347384	83459440	0.9387

Figure 10 Open area index for the west-east (a) and south-north (b) traverse for the base case

The open area index should also be checked in the *report* section of the *Terrain* module. The red line reflects the terrain profile in each direction (Figure 10). The difference between the min and max values for the open area should not exceed 10%. If the fraction between min and max value for the

open area becomes too small, blocking effects could lead to unphysical speed-ups similar to a wind tunnel.

3.5.2 Wind Fields Module

With a complete 3D terrain model from the *Terrain* module the simulation of the wind fields can be prepared. By solving the Reynolds Averaged Navier-Stokes equations the WindSim software calculates the wind fields. The turbulence model is set to the "*Standard k-epsilon*".

3.5.2.1 Boundary and initial conditions

The relevant sector for the chosen site is sector 330, based on the main wind direction from the provided measurement data. In the *Wind Fields* module, the sector input is set to "*manually set sector angles*" and "*sectors for next run*" to 330 (Figure 11).

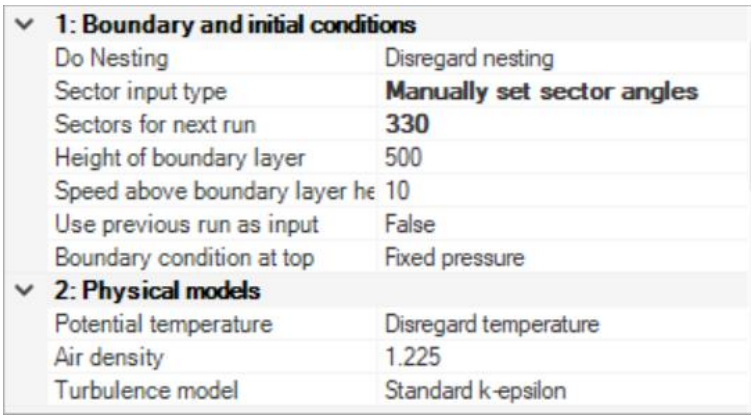

Figure 11 The properties settings for the Wind Fields module in the WindSim Software interface

The "*Height of the boundary layer*" is set to the default value of 500 meters, with a "*speed above boundary layer height*" of 10 m/s. With these settings the log profile is defined from the ground up to the height of the boundary layer. Above the set height the profile is constant, and the wind speed is persistent at the default value of 10 m/s.

3.5.2.2 Physical models

For all simulations in this thesis the "*Potential temperature*" is disregarded. The air density is set to the default value 1.225 [kg/m3] and as previously mentioned the "*Turbulence model*" is set to Standard k-epsilon.

3.5.2.3 Iterations and convergence criteria

The number of iterations is set to 800 with a convergence criteria of 0.0005. If the individual residuals drop below the value of the convergence criteria, the simulation will stop automatically. For some of the cases the convergence criteria might not be met after 800 iterations. In this case the residual values

are checked in the Wind Fields reports to make sure the plot is evening out (Figure 12). If the reported residual values are not satisfying after 800 iterations, the number of iterations will be increased. If more iterations are required WindSim offers an option of "*use previous run as input"*, which enables the user to continue the iterations from where it cut off.

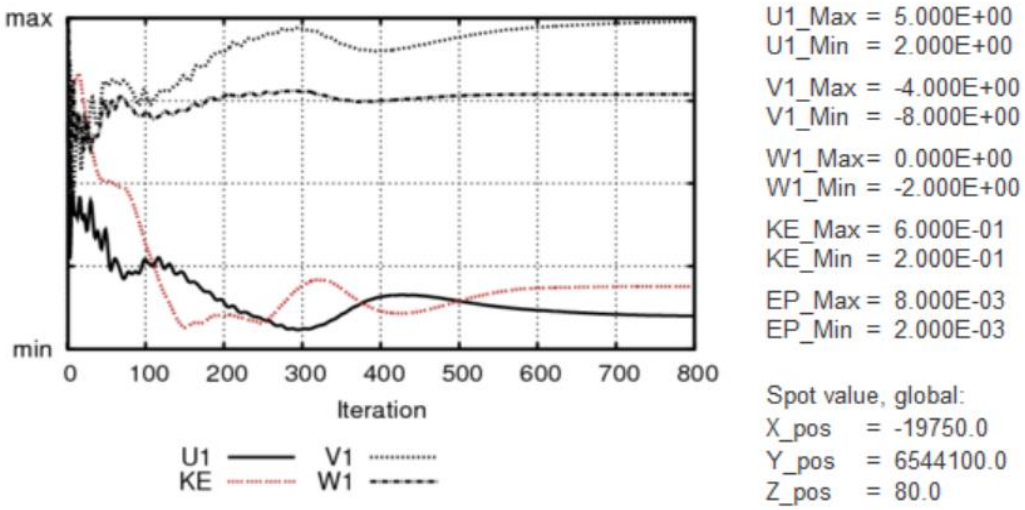

Figure 12 The spot value for the residuals displayed in the report section of the Wind fields module in the WindSim interface

3.5.3 Objects Module

The WindSim *Objects* module is used to place objects in the 3D terrain model, such as turbines and climatology. For this study the *Objects* module only contains turbines.

3.5.3.1 Turbine Positions

The position of turbines has been determined from the three met mast locations, respectively Nevlandsheia (*M1)*, Holmafjellet (*M2*) and Holmavatnet (*M3*). Turbines are placed approximately every 850 m in a triangular line between the three met masts (Figure 5). The distance between turbines is chosen in regard of a reasonable total number of turbines. The placement of the wind turbines is performed in Google Earth Pro (Google, 2021) with coordinates for every turbine transformed to the WindSim UTM 33 and then manually put into the WindSim *Objects* module (Figure 13). The wind turbines are placed in the model to obtain vertical profiles for the specific positions. The vertical profiles are the results and will be interpolated, filtered, and put into charts to be presented in the *Results* chapter. From these results the changes in the simulated wind fields will be analysed and discussed.

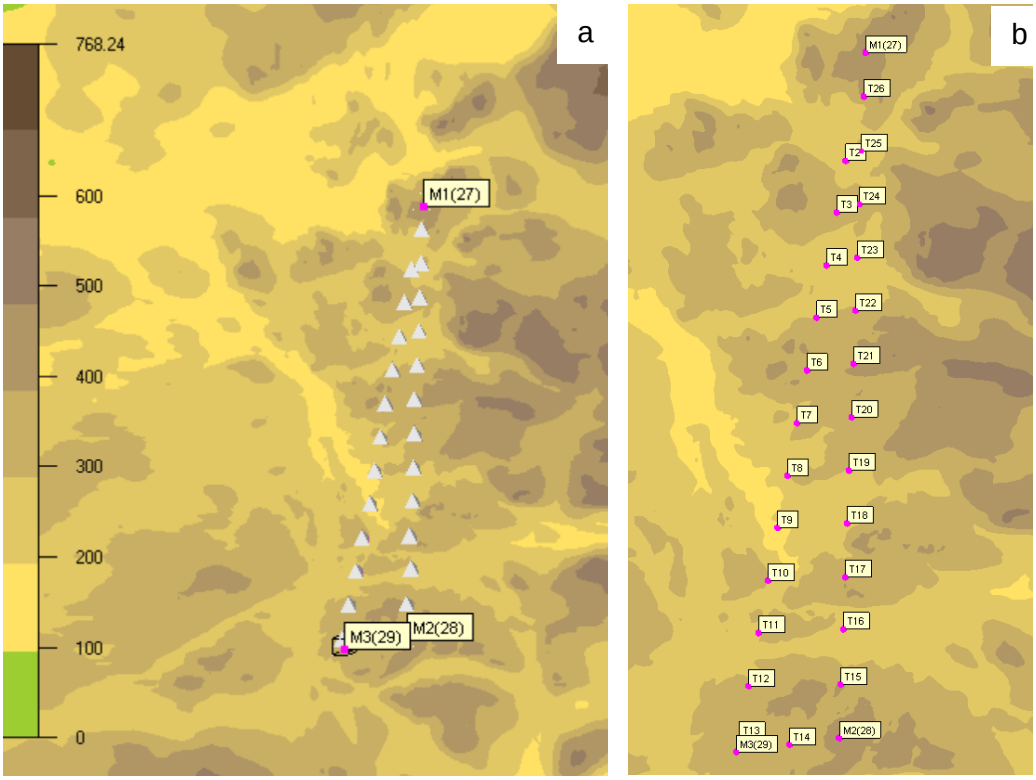

Figure 13 All turbines placed in the WindSim Objects module 3D viewer; the triangles are the turbines in the 3D viewer (a). Turbine positions and names (b). The legend shows the terrain elevation

3.5.3.2 Objects

As previously mentioned, the objects in this thesis consist solely of turbines. The turbines are named from T2 to T26 with their coordinates manually plotted into the "*Position*" tab in the *Objects* module. The three met masts are also put in as turbines, respectively *M1*, *M2* and *M3*. All objects have the same properties; hub height 80m, rotor diameter 90m and "*Terrain complexity calculation*" set to "*True*" (Figure 14).

1: Object definition	
Object type	Turbine
Name	**M1(27)**
Visualisation file	**turbine_80**
Power curve	**dummy_2000**
Hub height	**80**
Rotor diameter	**90**
Rotation speed	10
Facing wind direction	180
2: Position	
Coordinate system	**Global**
X position	**-18723.808**
Y position	**6549673.897**
3: Noise calculation	
Noise calculation	Disregard
4: Terrain complexity calculation	
Terrain complexity calcula	True

Figure 14 Objects module properties settings

The steps above are only necessary for the first case. After placing all turbine positions manually, the objects can be saved as an *.ows* file and thus imported to the other cases, as the turbines positions are equal for all cases in the study.

After running the *Objects* module, the vertical profiles can be exported as a *.txt* file (Figure 15).

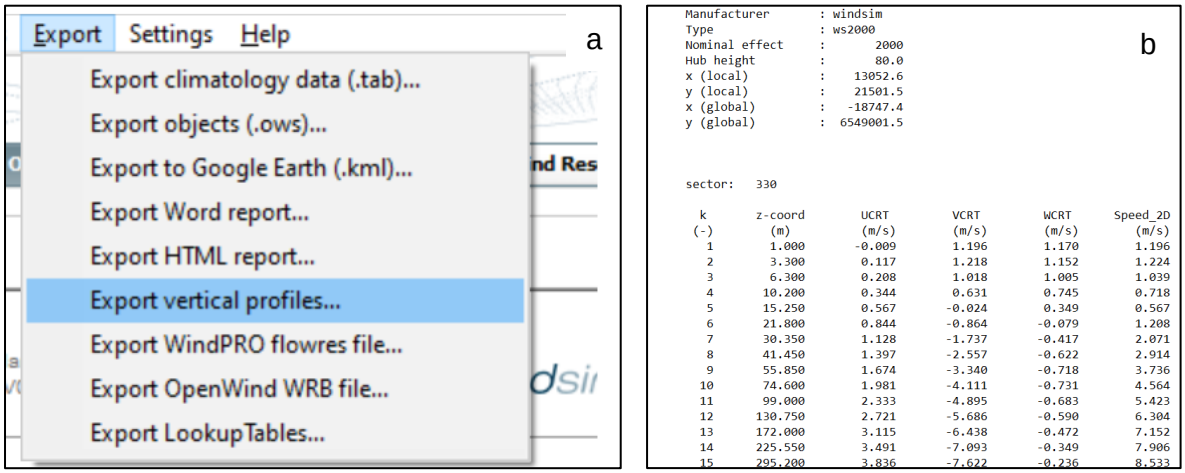

Manufacturer : windsim
Type : ws2000
Nominal effect : 2000
Hub height : 80.0
x (local) : 13052.6
y (local) : 21501.5
x (global) : -18747.4
y (global) : 6549001.5

sector: 330

k (-)	z-coord (m)	UCRT (m/s)	VCRT (m/s)	WCRT (m/s)	Speed_2D (m/s)
1	1.000	-0.009	1.196	1.170	1.196
2	3.300	0.117	1.218	1.152	1.224
3	6.300	0.208	1.018	1.005	1.039
4	10.200	0.344	0.631	0.745	0.718
5	15.250	0.567	-0.024	0.349	0.567
6	21.800	0.844	-0.864	-0.079	1.208
7	30.350	1.128	-1.737	-0.417	2.071
8	41.450	1.397	-2.557	-0.622	2.914
9	55.850	1.674	-3.340	-0.718	3.736
10	74.600	1.981	-4.111	-0.731	4.564
11	99.000	2.333	-4.895	-0.683	5.423
12	130.750	2.721	-5.686	-0.590	6.304
13	172.000	3.115	-6.438	-0.472	7.152
14	225.550	3.491	-7.093	-0.349	7.906
15	295.200	3.836	-7.622	-0.236	8.533

Figure 15 Exporting the vertical profiles after running the Objects module (a). Vertical profile .txt example (b)

3.5.4 Results Module

The final step in the WindSim software is the *Results* module. In this module 2D Velocity Vector XY- and 2D Speed Scalar XY- plots are generated from the *Wind Fields* module simulation results. These plots present the wind speed vector and -scalar in the horizontal plane for the relevant sector angles, in this study sector 330. The height above ground level for which the results should be generated is specified, and multiple heights can be given, e.g., 19, 49 and 100m.

3.6 Data Filtering

The vertical profiles for every single case are exported from the *Objects* module as a *.txt* file.
A variety of solutions exist for filtering and extracting the data of interest. In this study Microsoft Excel is used to transform the vertical profiles and extract the 2D wind-speeds. The vertical profile contains the wind speeds at different heights for every wind turbine position in every case. All data sets need to be filtered, sorted, and then presented in the results.

3.6.1 Vertical Profiles

From the measurement data it can be seen that the met masts measure the wind speed at heights 19, 33 and 49m, where 19 and 49m will be used to validate the speed ups in the simulations. To validate the results the simulated 2D wind speeds in the vertical profiles exported from WindSim need to be interpolated to match the reference heights. In the exported vertical profile *.txt* file (Figure 15) the *z-coord* row tells at which height above the terrain the wind speed is simulated.

WindSpeeds Height	T1	T2	T3	T4	T5	T6	T7	T8	T9
	Speed_2D	Speed_2D	Speed_2D	Speed_2D	Speed_2D	Speed_2D	Speed_2D	Speed_2D	Sp
	(m/s)	(m/s)	(m/s)	(m/s)	(m/s)	(m/s)	(m/s)	(m/s)	(m
1.00	1.20	3.482	1.526	3.04	3.839	2.78	2.174	3.404	
3.30	1.22	4.547	2.956	3.53	4.289	3.705	2.773	4.099	
6.30	1.04	5.038	3.638	3.646	4.451	4.124	3.082	4.391	
10.20	0.72	5.353	4.123	3.76	4.556	4.452	3.434	4.596	
15.25	0.57	5.589	4.461	3.889	4.671	4.778	3.829	4.799	
21.80	1.21	5.805	4.717	4.051	4.818	5.126	4.265	5.024	
30.35	2.07	6.033	4.933	4.263	5.009	5.495	4.733	5.279	
41.45	2.91	6.297	5.121	4.541	5.255	5.885	5.225	5.567	
55.85	3.74	6.6	5.298	4.896	5.555	6.3	5.723	5.881	
74.60	4.56	6.928	5.478	5.326	5.911	6.743	6.22	6.221	
99.00	5.42	7.255	5.68	5.809	6.323	7.212	6.706	6.583	
130.75	6.30	7.566	5.922	6.309	6.79	7.697	7.177	6.968	
172.00	7.15	7.859	6.227	6.809	7.312	8.174	7.635	7.375	
225.55	7.91	8.143	6.631	7.313	7.87	8.617	8.079	7.8	
295.20	8.53	8.435	7.182	7.834	8.42	9.014	8.509	8.235	
Height									
19	0.934	5.713	4.608	3.982	=FORECAST.LINEAR($A$21;F8:F9;$A$8:$A$9)				
49	3.345	6.456	5.214	4.727					
100	**5.451**	**7.265**	**5.688**	**5.825**					

FORECAST.LINEAR(x; known_ys; known_xs)

Figure 16 The vertical profile for every turbine is imported to excel and interpolated to match the reference heights of the met masts

The .txt vertical profiles are imported to excel and the 2D wind speed for every turbine is extracted and sorted in a methodical way. Figure 15 shows that the reference heights are not represented in the vertical profiles, this means an interpolation is needed to find the wind speed. In addition to the reference heights of 19 and 49m, height 100m is added to the table as this is a relevant height to wind turbine operation. Calculating the wind speed is done using the Excel formula: **[forecast.linear()]** on the two closest heights and wind speeds (Figure 16). This procedure is repeated for all 20 cases.

3.6.2 Normalizing the Wind Speed

The 2D wind speed for all cases is normalised to the reference point *M3* (Holmavatnet). The speed-up from *M3* to *M2* will be used to validate the simulated speed-up. By comparing the speed-up in the simulations to the measurement data it can be seen if there is a correlation. If the reference speed-up is negative between *M3* and *M2* and the simulated speed-up is positive, it can be assumed that the simulation data is not correct. To normalise the 2D wind speed all simulated results are divided on the *M3* value for the given height, leaving $M3 = 1$ for all heights and all cases. The reference speed-up from *M3* to *M2* will be included in the 19 and 49m bar-charts to be compared with the simulated speed-up for the given numerical setting. The data will be presented in bar-charts as it gives a clear presentation of the results, and the data can be visually compared. In addition to the bar-charts, vector plots and speed scalar plots in XY- direction from the WindSim *Results* module will be used to analyse the differences and variety for all cases in the next chapters.

4. Results

In this chapter the results from the vertical profiles for all numerical settings will be presented. Speed scalar plots from the WindSim *Result* module will be added to show differences between cases and to give a more thorough assessment of points of interest.

The bar-charts presented in this chapter shows the normalized wind speed at height 19, 49 and 100m above ground for all turbine locations predicted by the WindSim simulations. The numerical settings for *S1-S20* are defined in Error! Reference source not found. The Base Case (*S1*) is included in all charts and the measured speed-up at heights 19 and 49m above ground for turbine positions *M3* and *M2* is included in the relevant charts, respectively *Ref 19* and *Ref 49*.

4.1 Resolution

From Figure 17 the magnitude of difference between the numerical settings can be seen, and it varies from turbine to turbine. As an example, *T14* and *T6* have minor changes in the results with changes in horizontal resolution, while for *T26* and *T16* the normalized wind speeds changes in relation to the numerical setting. It's interesting to see that the greatest range of variation is between the highest and the lowest horizontal resolution. The three bar-charts display the normalized wind speeds for the respective heights 19, 49 and 100m above the terrain. From the three bar-charts the greatest variations in wind speeds between numerical settings and turbine positions is occurring closest to the terrain. This is because the terrain has more impact on the wind flow closer to the ground. Further on as the simulated height is increased the range of variation is reduced both between turbine positions and numerical settings.

Figure 17 Normalized wind speed for all turbine positions in cases S2-S6. Displayed here for heights 19 (a), 49 (b) & 100m (c) above the terrain

The wind speed graphics from the WindSim *Results* module displays the wind speed for the different heights in the numerical settings. Presented in the Figure 18 and Figure 19 is the speed scalar 2D wind speed for numerical setting *S2* and *S6* at height 19, 49 and 100m above ground. From the speed scalar graphics, it can be seen there are major differences in the simulated wind speed. It's interesting to notice that the variation is great even at 100 meters height. By inspecting the speed scalar graphics it's possible to get a closer understanding of the normalized wind speed variations presented in Figure 17. The wind speed legend shows that the higher resolution model, *S2*, has higher simulated maximum wind speed and lower minimum wind speed for all heights compared to the lowest resolution model *S6*.

As the simulated height in the model increases, the wind flow is less turbulent. This relates to the impact of the terrain on the wind flow, the further above the terrain the less influence the terrain has on the wind flow.

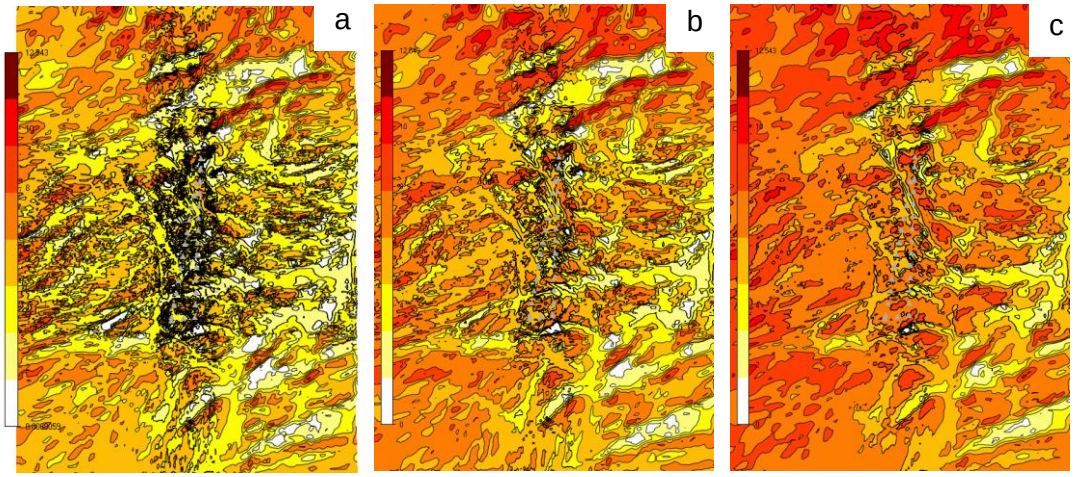

Figure 18 The simulated wind speeds at 19 (a), 49 (b) & 100m (c) above ground for numerical setting S2

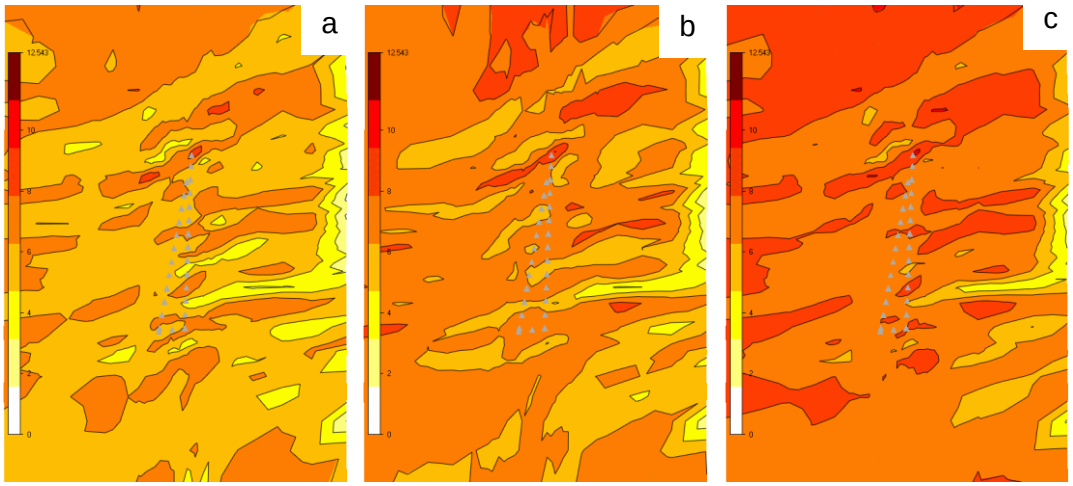

Figure 19 The simulated wind speeds at 19 (a), 49 (b) & 100m (c) above ground for numerical setting S6

4.2 Domain

The Figure 20 displays the normalized wind speeds of the cases containing different values for the size of the simulation domain. The representative heights are 19, 49 and 100m above ground level. The range of domain sizes is given in the numerical setting matrix (Table 2). From the charts it can be seen that the variation in wind speed is not as gradually distributed as for the resolution numerical setting. Where the difference between cases increased proportionally with the number of cells for the resolution cases, this does not seem to be the case for the domain size setting. An interesting point is that the variation in wind speed for the different domain sizes remains stable as the simulated height is increasing. Additionally, there is little change in results for the three cases with the largest domain buffers. This indicates that by further increasing the model size, the impact of the additional

peripheral terrain does not have a significant impact on the results of the model. Therefore, the influence of the terrain outside the 20km buffer can be regarded as negligible. It is worth noting that the greatest variability occurs for the cases with a 5 and 10km domain buffer (*S9* and *S1*). The reason for this spike in wind speed for the medium sized models will be analysed in the *discussion* chapter.

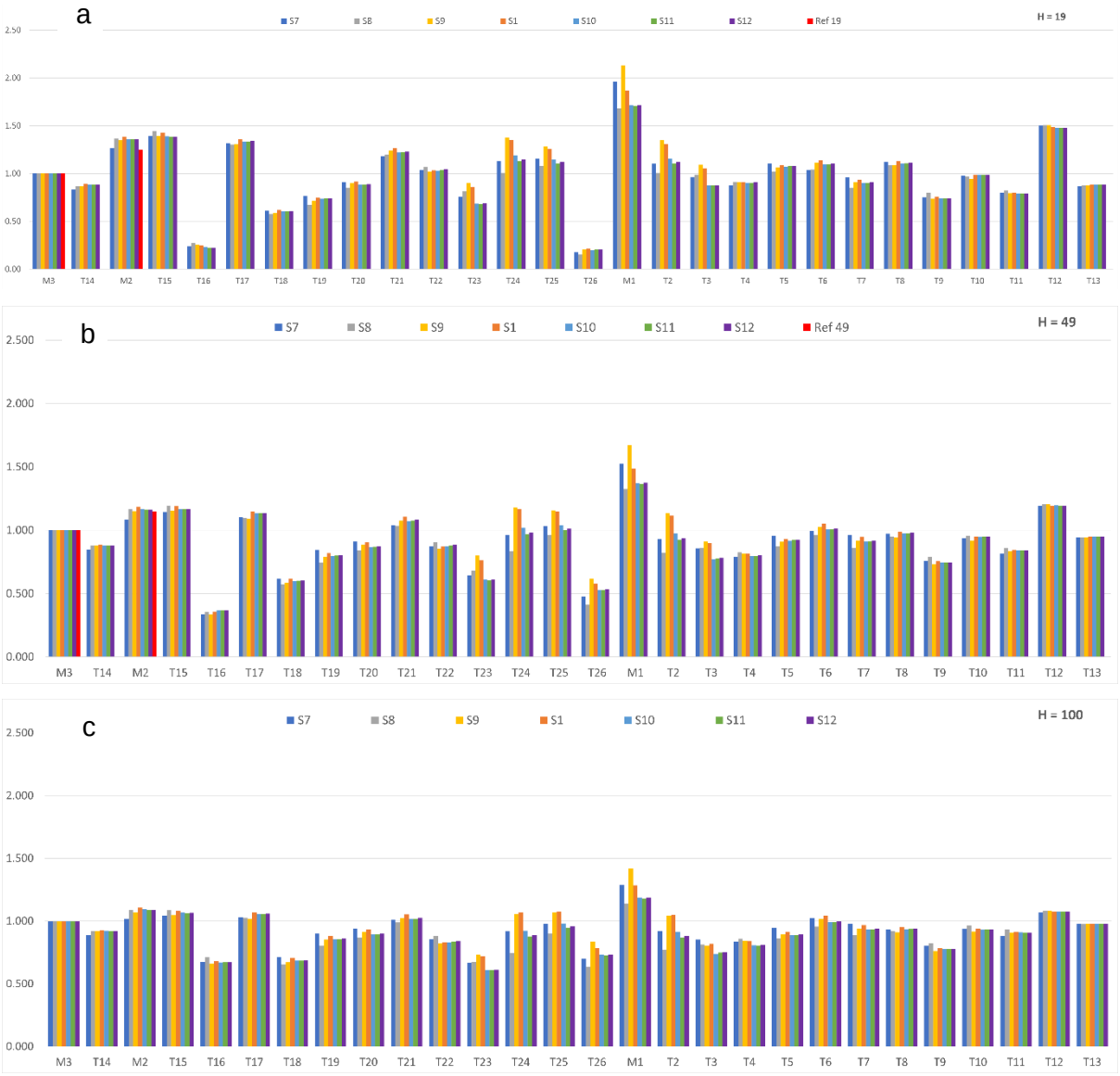

Figure 20 Normalized wind speed for all turbine positions in cases S7-S12. Displayed here for heights 19 (a), 49 (b) & 100m (c) above the terrain.

The below speed scalar plots from the WindSim *Results*-module shows the simulated wind speed for numerical setting *S7* (Figure 21) and *S12* (Figure 22) at heights 19, 49 and 100m above the terrain. Obviously the *S12*-case with a domain buffer of 30 km covers a larger area than the *S7*- model with a domain buffer of 1 km.

The model with a 1 km domain buffer produces a narrow model where the inflow area prior to the turbine area is very limited. It can be assumed that this small buffer zone restricts the development of the wind flow and wind profiles, and thus the flow will not be sufficiently evolved. The models with larger domain buffers cover a great peripheral area of the wind farm where the wind flow can fully mature in advance of entering the turbine area. These assumptions will be further analysed and discussed in the next chapter.

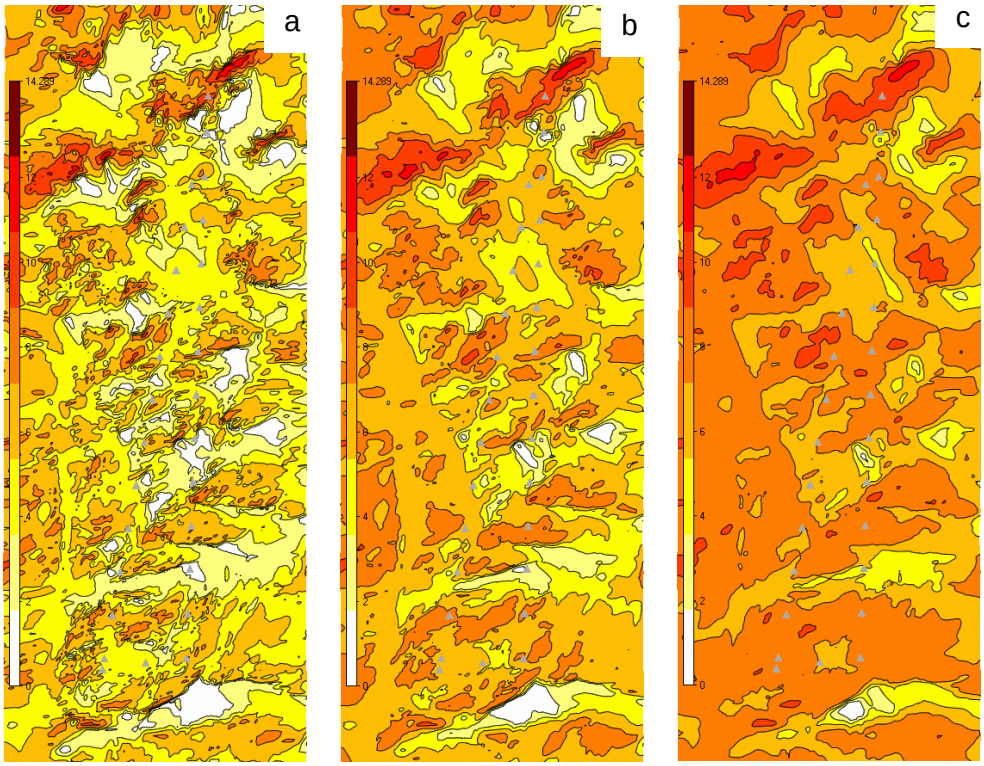

Figure 21 The simulated wind speeds at 19 (a), 49 (b) & 100m (c) above ground for numerical setting S7

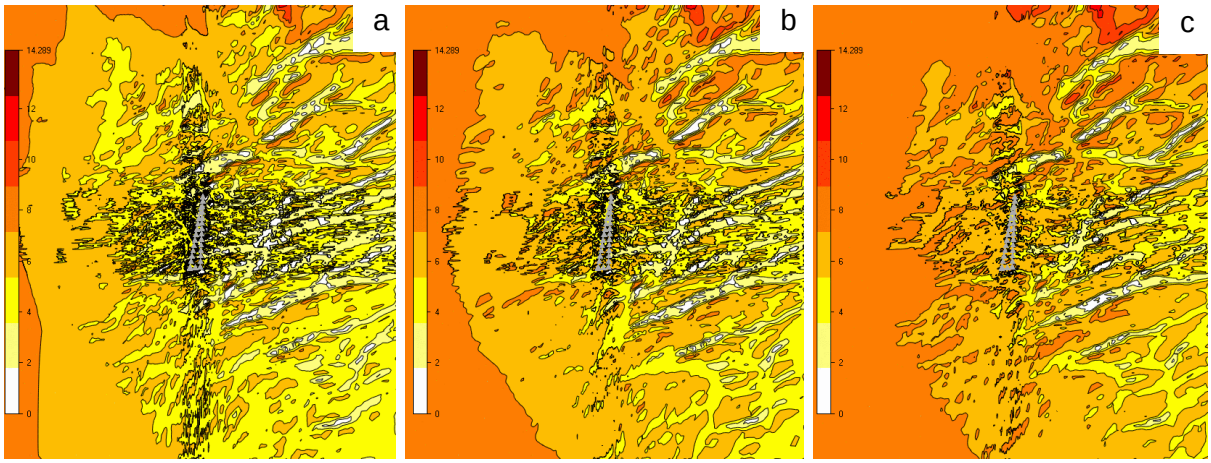

Figure 22 The simulated wind speeds at 19 (a), 49 (b) & 100m (c) above ground for numerical setting S12

4.3 Refinement Area

The third numerical setting is the size of the refinement area. The Figure 23 presents the results for the models with different sized refinement areas as defined in the numerical setting matrix (Table 2). Though the differences in wind speeds are not massive there is a trend with a few exceptions, toward higher wind speed as the refinement area is increasing. The pattern consists for the respective simulated heights.

Figure 23 Normalized wind speed for all turbine positions in cases S13-S17. Displayed here for heights 19 (a), 49 (b) & 100m (c) above the terrain

The graphics below shows the simulated wind speeds for the two cases with refinement areas of respectively 0 km (Figure 24) and 7 km (Figure 25). The model with 0 km (*S13*) still contains a refinement area, but it's fitted to the exact extension of the turbine area and has a total of 2 million cells. The model with the largest refinement area (*S17*) consists of 19,6 million cells and the refinement area covers close to the whole model. From the wind speed graphics, the difference in detail is significant. As the wind flow advances through the model, it can be assumed that the development of the flow is more accurate for the higher resolution model. These assumptions will be further analysed in the next chapter.

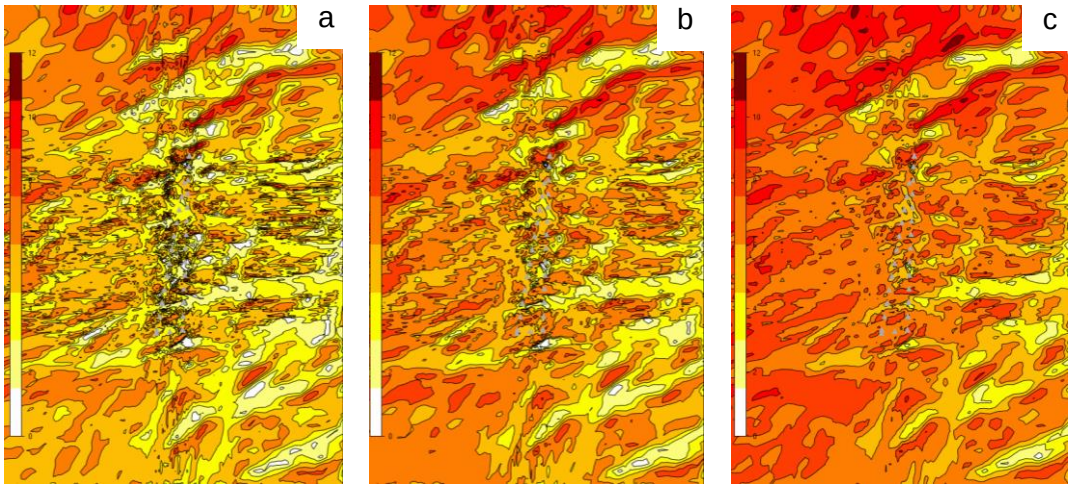

Figure 24 The simulated wind speeds at 19 (a), 49 (b) & 100m (c) above ground for numerical setting S13

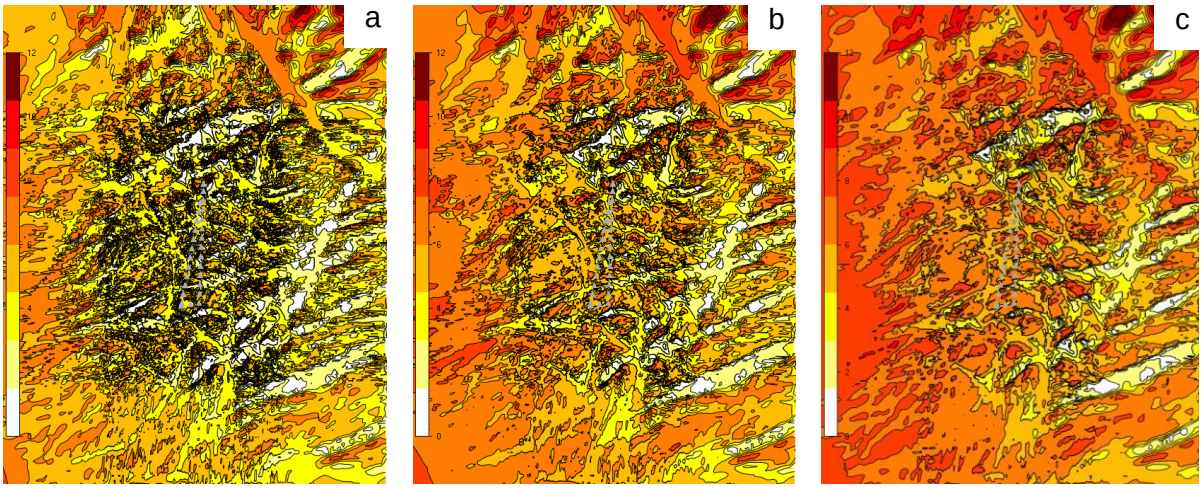

Figure 25 The simulated wind speeds at 19 (a), 49 (b) & 100m (c) above ground for numerical setting S17

4.4 Vertical Distribution

The vertical distribution involves the number of layers in the z-direction in addition to the positioning of the layers. The vertical levels in the cases of this study are distributed in a geometric setting as shown in the *Methodology* chapter. The bar-charts shows the normalized wind speeds for the cases

with different number of layers in the vertical. From the charts (Figure 26) it can be seen that the largest differences are occurring between the cases with the biggest difference in number of cells and layers. The blue bar displaying the *S18* case with 10 layers in the vertical is for most turbine positions the biggest polarity to the yellow bar of the *S20* case with 50 layers in the vertical. As observed from previous charts the difference between wind speed for the turbine positions decreases as the simulated height is increasing. Still the distinct gap between the numerical settings persists for every position.

Figure 26 Normalized wind speed for all turbine positions in cases S18 - S20 at 19 (a), 49 (b) & 100m (c) above the terrain

From the wind speed graphics, the differences in simulated wind speed for the two numerical settings *S18* (Figure 27) and *S20* (Figure 28) can be observed. The 10-layer vertical case (*S18*) shows higher wind speeds throughout the domain in a less detailed model. From the graphics it looks like the terrain

has a greater influence on the simulated wind flow for the *S20* case with 50 vertical layers. The areas of low wind speed are more dominant and areas of high wind speed more concentrated in the high-resolution case.

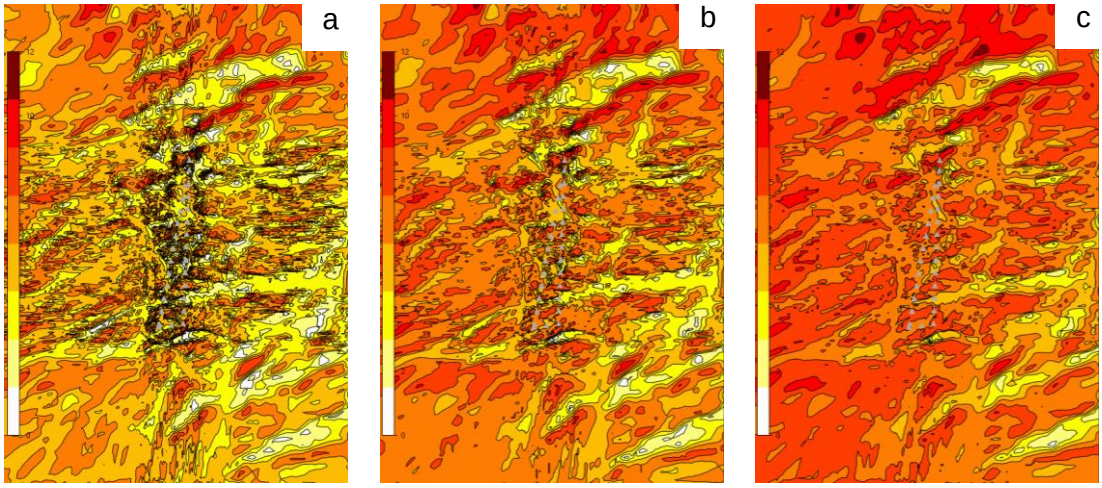

Figure 27 The simulated wind speeds at 19 (a), 49 (b) & 100m (c) above ground for numerical setting S18

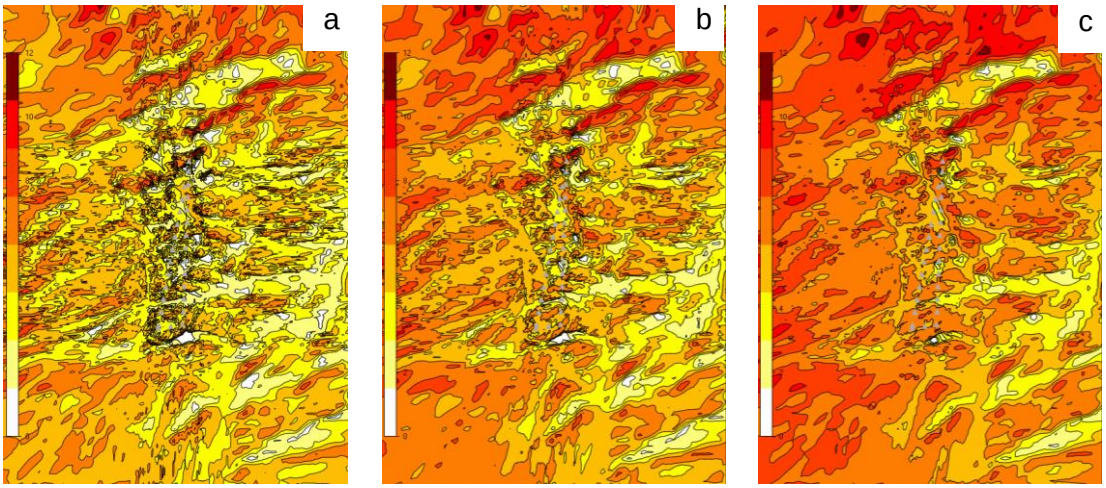

Figure 28 The simulated wind speeds at 19 (a), 49 (b) & 100m (c) above ground for numerical setting S20

4.5 Summary Presentations

From the charts and graphics presented, an overview of the differences in wind speed between cases and heights has been established. Variations of interest have been pointed out and will be further investigated in the discussion chapter. From the charts it can be seen that for certain turbine locations such as *T16*, *M1* and *T26* the predicted wind speeds are very different between the numerical settings. Specific turbine positions, cases, and points of interest will be further analysed and discussed in the next chapter. Investigating grid dependency, terrain variations and low wind speed areas with potential recirculation zones will be prioritized.

5. Discussion

In this chapter the results presented in chapter 4 will be assessed and analysed. In an attempt to keep the data and assessment comprehensible the sub-chapter structure from the previous chapter will be maintained. Meaning the different numerical settings will be discussed separately with a focus on internal differences between the selected numerical values. A comparison between the numerical settings will be included if deemed relevant towards the end of the chapter.

5.1 Resolution

From the results for the different resolution models there is a solid trend in the bar chart. For close to every turbine location the variety in the simulated 2D wind speed between the cases with highest and lowest resolution is substantial. Knowing the great gap in resolution for the two models it is fair to assume the terrain topography is not sufficiently reproduced in the coarser model. From the graphics (Figure 29) the green turbines represent higher simulated wind speed-ups for the *S2* model, while the yellow turbines are locations where the wind speed-up for *S2* are higher at lower heights but equals out as the simulated height is further above ground. These locations are on hills and ridges, and it can be assumed that the simulated speed-up in the *S2* case is greater than the speed-up for the *S6* case, at least closer to the ground, but as the height increases the impact of the terrain on the wind speed is less significant (Carpenter and Locke, 1999). Higher speed-up is related to the topography and complexity of the terrain, a closer examination of the velocity plots shows that coarser grids tend to slightly underestimate the speed-up (Abdi and Bitsuamlak, 2014). Because models with coarser grids do not accurately reflect the landscape, mountains, hills, and mounds are levelled, some of its extreme characteristics are lost. As previously mentioned, a higher resolution model results in higher maximum wind speeds and lower minimum wind speeds. The white-labeled turbines refer to the positions where the *S6* model simulates the higher wind speed-ups. In Figure 29 it can be seen that these positions are in general on the lee side of elevations in the terrain. The low wind speed zones in the high-resolution model are not reproduced in the low-resolution model and thus the wind flow is not affected by the hills and ridges in a similar way (Castro et al., 2003). Recirculation zones form on the lee side of these terrain features if they are steep enough. Large wake zones extend behind the ridges and mountains where there is a substantial velocity loss, which can stretch for multiple hill heights behind the top (Stangroom, 2004). The recirculation zones in *S2* are further developed than in the cases with lower resolution as seen in Figure 30 and Figure 31. There looks to be a larger low wind speed zone on the lee side of the ridge just north-northwest of the *M1* turbine in the *S2* case which could potentially explain the lower simulated wind speed. In addition, the recirculation zone on the lee side of the Nevlandsheia hill is further developed in *S2*, and it could be speculated that this could cause the hill to act more like a plateau and thereby reduce the speed-up.

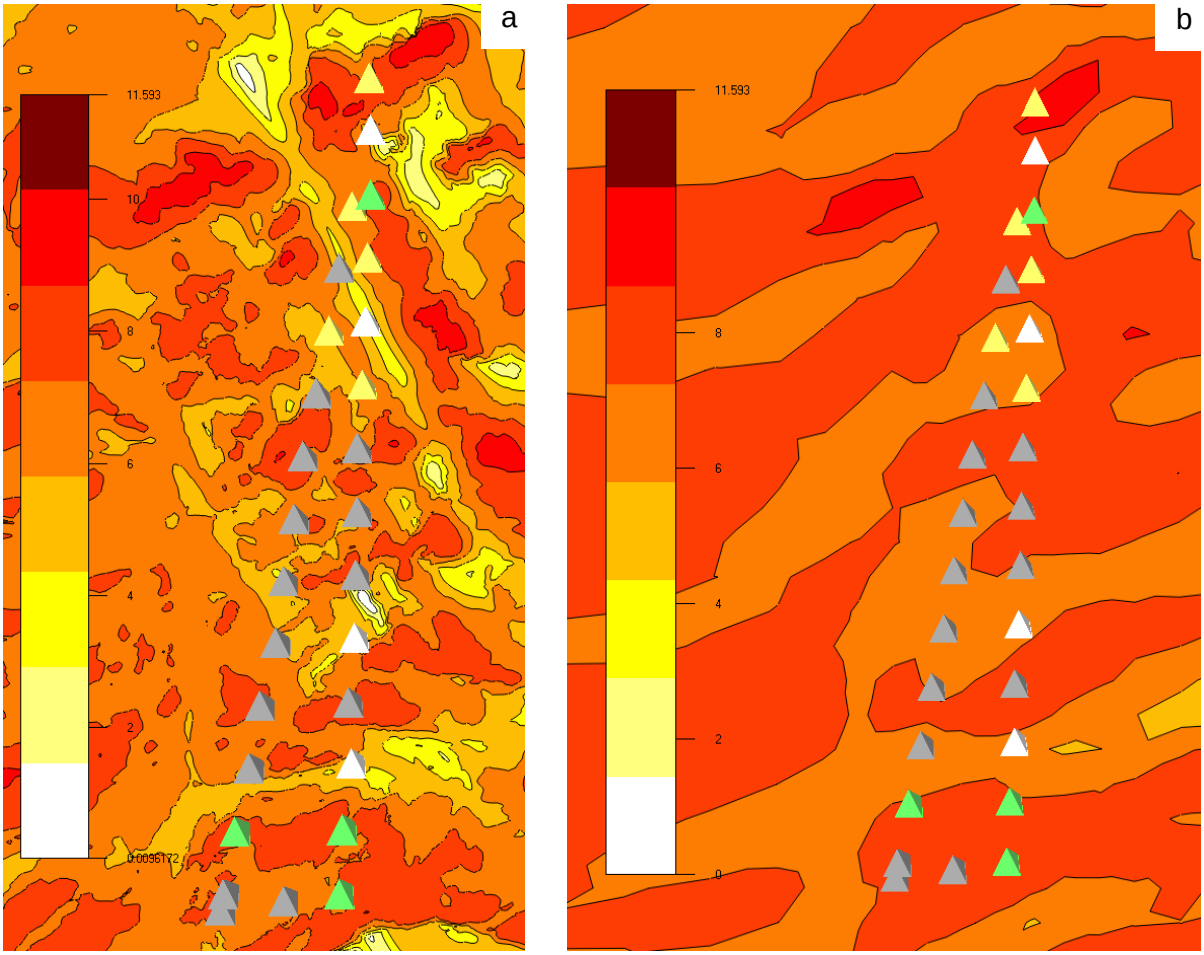

Figure 29 Comparison of numerical setting S2 (a) and S6 (b) at height above terrain, H = 100. Green turbines represent higher simulated wind speed-ups for the S2 case. Yellow turbines represent higher simulated wind speed-ups for S2 at lower heights but equals out further above ground. White turbines have highest simulated wind speed-ups for the S6 case

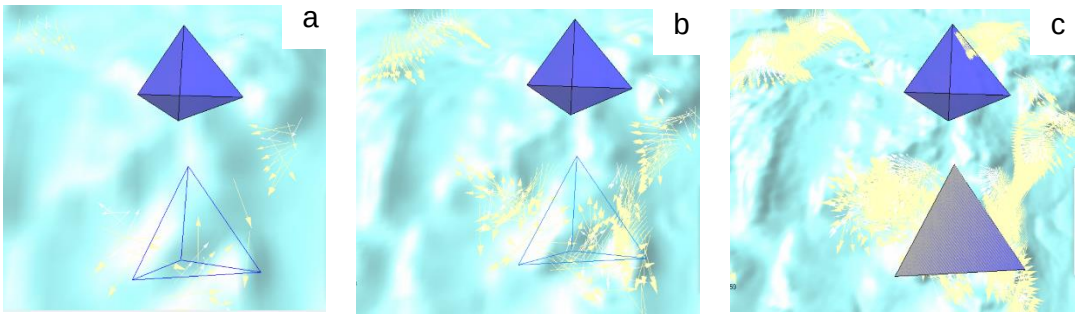

Figure 30 Vector plots for wind speed from 0-1.2 m/s in cases S3 (a), S1 (b) & S2 (c) with a resolution of 50x50, 25x25 and 10x10 meters respectively. The vectors show that the wind is moving in multiple directions and the largest recirculation zone is clearly in the high-resolution model (c). Height above terrain, H = 19

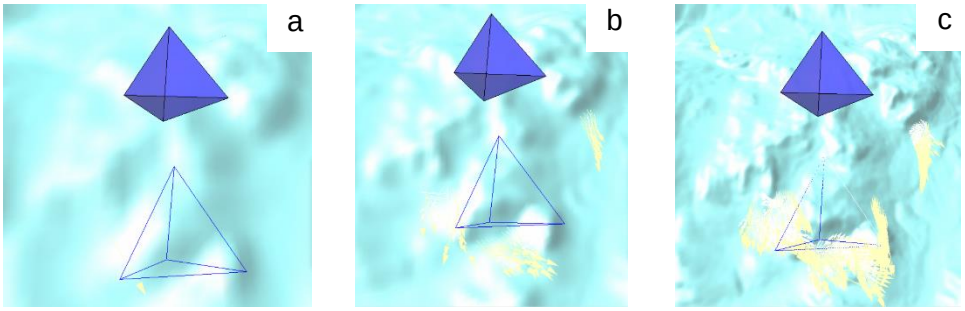

Figure 31 Vector plots for wind speeds 0 - 1.2 m/s in cases S3 (a), S1 (b) & S2 (c) with a resolution of 50x50, 25x25 and 10x10 meters respectively. The recirculation zone is close to absent in S3 (a), but still very visible in S2 (c). Height above terrain, H = 49

The mapping of areas of low wind speed and recirculation is as important as finding the areas of high wind speed with respect to turbine placement. The coarsest model in this study shows no sign of recirculation zones and areas of low wind speed is close to absent. From Figure 32 the formation of the low wind speed zones on the lee sides of hills and ridges starts occurring gradually from a resolution of 200m (*S5*) at a height of 100m above ground. It can be argued that to obtain satisfying simulation results, a proper reproduction of areas of low wind speed and recirculation is desired, and thus a mesh grid of the highest possible resolution should be selected. There is a noticeable difference between the *S2* and *S1* for the majority of turbine locations, which indicates that grid independence is not achieved when increasing the resolution of the grid from 25 m to 10m. The simulation results in this study are still sensitive to changes in grid resolution and it can be assumed that further increasing the resolution might provide even more accurate results.

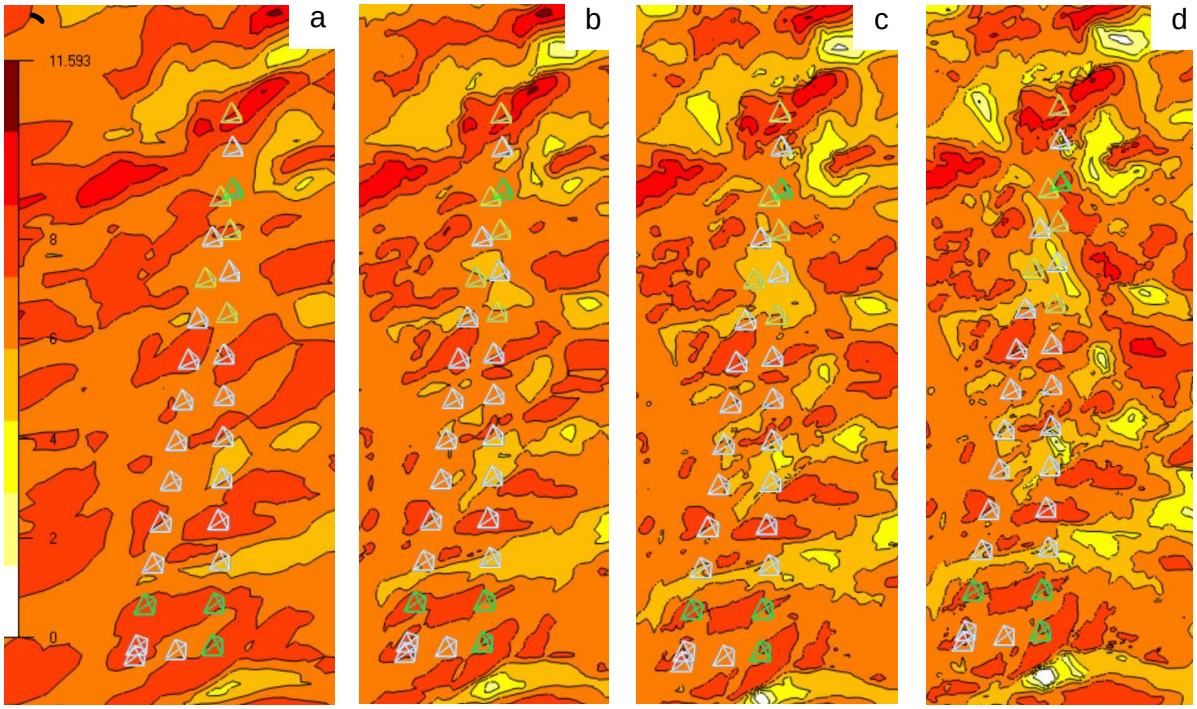

Figure 32 Development of low wind speed zones at 100m above the terrain for models S5 (a), S4 (b), S3 (c) & S1 (d)

5.2 Domain

The *domain* results show no clear correlation between number of cells and simulated wind speed. Compared to the other parameters, the difference between cases is not proportionally to the number of cells for the domain buffer size parameter. A noticeable trend in the bar-charts were the *S9* and *S1* models showing spikes in simulated wind speed for several turbine positions. These spikes in wind speed are occurring for turbines located in the northern part of the wind farm. The wind field simulations in this study are done with an inflow direction from sector 330 i.e., the wind direction is from north-northwest. By investigating the terrain conditions close to the border in the two deviating models, a better understanding of the reason can be established. The displayed horizontal wind speed graphics in Figure 33 shows the highest wind speed occurs in the northern part of the model, in the area closest to the inlet wind direction. By comparing the *S1* and *S9* models to the *S10* it seems the limited domain buffer of the two smaller models has a great influence on the simulated wind speed upstream the wind farm. From Figure 33 the horizontal wind speed in the boxed-in ridge is in the range of 11-14 m/s for cases *S9* and *S1*. In comparison the wind speed over the ridge for case *S10* is in the range of 7-9 m/s.

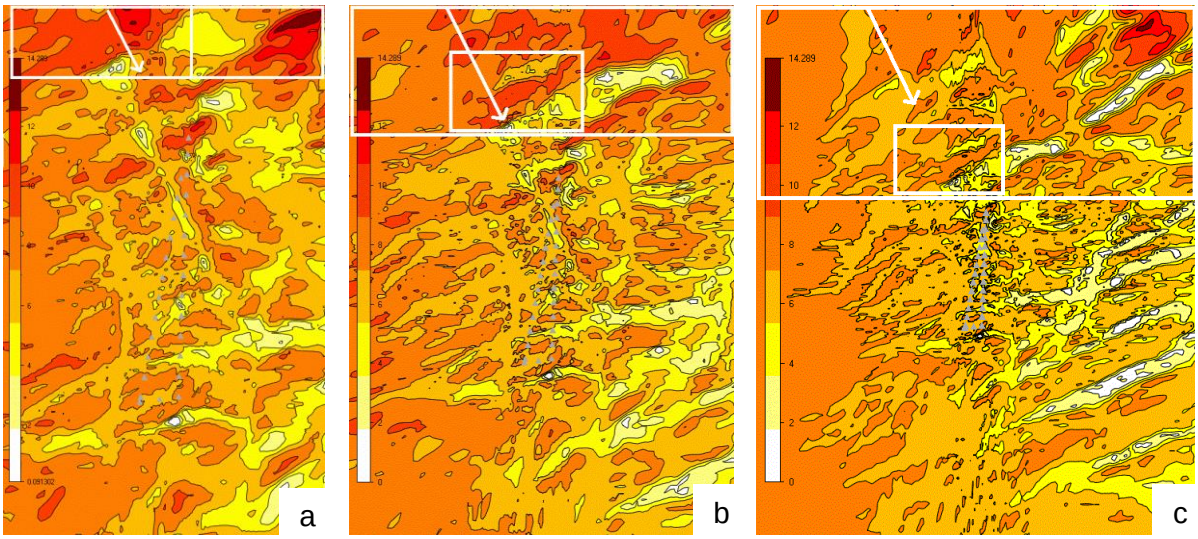

Figure 33 The simulated horizontal wind speed for S9 (a), S1 (b) & S10 (c). The marked area is highlighting the ridge/hill upstream the wind farm. The white arrow resembles the inlet wind direction. Height above terrain, H =100

As previously stated, the simulated wind direction is from north-northwest and the boxed-in ridge in Figure 33 is close to perpendicular to the upstream wind flow. The wind flow at the boundary is set to 10 m/s and the speed-up on the marked ridge has a great influence on the flow as it enters the wind farm. For *S9* the ridge is close to the boundary, and this results in an artificial speed-up close to the wind farm (Dhunny, Lollchund and Rughooputh, 2017). The increased domain buffer for the *S1* model still contains hills and ridges close to the border with high speed-up factors and the influence on the simulated results is similar to the *S9*. Increasing the domain buffer to 20km as in the *S10*

model, the terrain upstream of the wind farm is extended and the specific ridge has less impact on the simulated wind flow as it approaches the turbines. The wind flow is allowed to fully develop with the large buffer without artificial speed-ups close to the boundary. It can be argued that the limited domain buffer for the *S9* and partly *S1* causes the particular ridge to act more like an isolated hill in the terrain upstream the turbines. Miller and Davenport (1998) showed through their work that velocity speed-ups in complex terrain with several hills in series are reduced compared to those found on isolated hills. Hills in series dulls the terrain effect and make the hills act almost like a very rough surface. It can be assumed that the combination of the ridge being a stand-alone terrain feature in addition to being close to the border, not letting the wind flow properly develop, causes the wind speed to spike for the *S9* and *S1* cases. The result bar-charts show that increasing the domain buffer beyond 20km has close to no impact on the results and it can be argued that domain buffer grid independency is reached at 20km.

Alternative methods to expanding the domain exists. *Smoothing* is a method where the terrain in parts of the model is smoothed. The method can be used to smoothen the terrain in the outer part of the model, towards the border, to change the height of the terrain and preventing artificial speed-ups close to the boundary. By applying the method only to the outer part of the model, the areas of interest at the centre of the model are not affected directly, but indirectly by the reduced influence of the complex terrain upstream (Montavon et al., 2009)**.** A second option is the *Nesting* technique which involves using the results from a larger 3D model that cover the current smaller 3D model. The wind profiles at the boundaries and the initial conditions are interpolated from the larger 3D model. The previously run big model can be a WindSim model or a mesoscale meteorological model. The nesting method reduces the inaccuracies introduced by applying the log profiles.

5.3 Refinement area

When altering the size of the refinement area in a model the area of maximum resolution in the model changes. An increase from e.g., 1 km to 2km, expands the area where high resolution and accurate results is obtained. This results in a huge increase in number of cells and thus strongly affects the simulation time. From analysing the bar-charts in the results chapter it is observed that the step-by-step expansion of the refinement area has a limited impact on the simulated results. There is but a slight trend towards higher simulated wind speed when increasing the refinement area size and number of cells, with a few exceptions. The *S1* case shows a spike in simulated wind speed for the turbines *T2, T24* and slightly *T25,* all located on the lee side of the Nevlandsheia-hill in the northern part of the turbine area. For the same three turbines the *S16* model has, unexpectedly, significant lower simulated wind speeds than the rest. There is also a noticeable spike in the wind speed for the *T3* and *T23* turbines in case *S16*. Turbines *T3* and *T23* are positioned in the valley behind the

Nevlandsheia-hill in line with the simulated wind direction, just west of the three other relevant turbines. By investigating the placement of the refinement area border for the *S16* and *S1* cases there might be an indication to why the wind speed diverges this much between the cases at turbines *T2*, *T24* and *T25*.

In Figure 34 the 2D wind speeds and horizontal grids for cases *S1* and *S16* are displayed. The areas of high cell density are the refinement areas. From the graphics the placement of the refinement area borders can be seen and for the *S1* the northern border is placed mostly in a valley where the wind speed is relatively low. The northern border of the *S16* case refinement area is placed on top of the mountain ridge north of the wind farm. The two points marked in the wind speed maps shows the wind speed and elevation. The difference between the simulated wind speeds is significant, both at the top of the mountain ridge and at the floor of the valley further south. Clearly the *S16* case has a larger developed low wind speed area on the lee side of the ridge which could explain the discrepancies between the two cases.

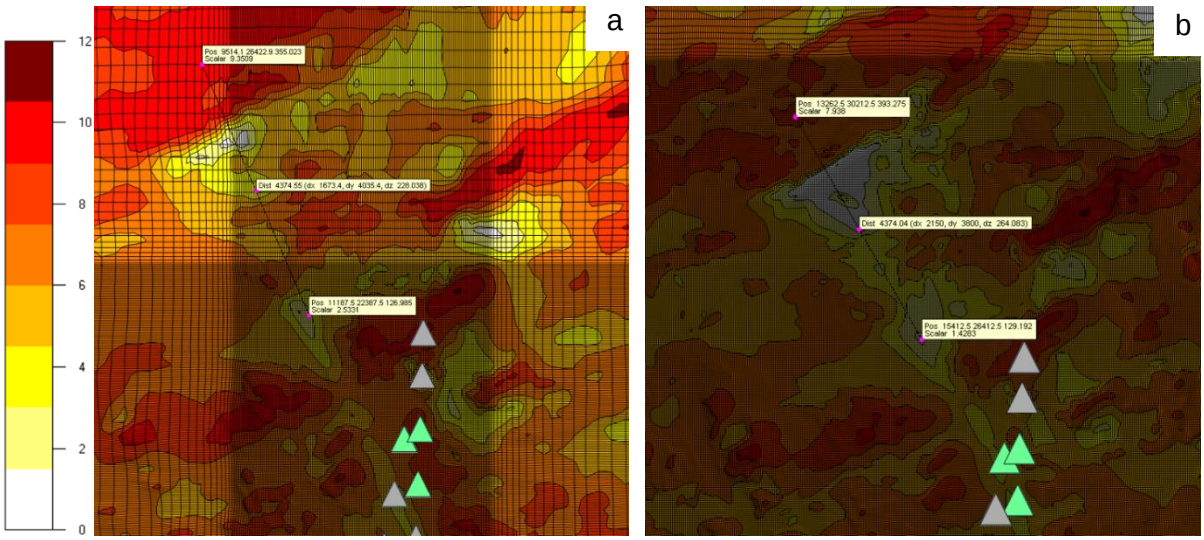

Figure 34 2D wind speed graphics for the S1 (a) and S16 (b) with the grid displayed. The green turbines are T25, T2 and T24 (North to South). Scalar value is the simulated wind speed at the height above terrain H = 100

The terrain just north of the turbines towards the inlet wind direction, is investigated in Figure 35. The highlighted points in the graphics show the differences in wind speed over the Nevlandsheia-hill and in the valley on the lee side. The *S17* case has been included as comparison, as it follows the trend in the bar-charts and show no signs of unexpected results for any turbine positions. The points highlighted in the graphics shows the wind speed over the ridge on the west side of the Nevlandsheia-hill and the wind speed on the lee side close to the turbines. The difference observed at these points reflects the discrepancies in the bar-charts. It also reflects the difference in simulated wind speed at the points in Figure 34 and the origin could debatable be the placement of the northern refinement area border. The two turbines marked with black outline in Figure 35 are *T3* and *T23*, where the

simulated wind speed for case *S16* spikes. Based on the data available at this time it can only be assumed that the difference in the wind field at this location is occurring for the same reasons as the differences at the other two locations.

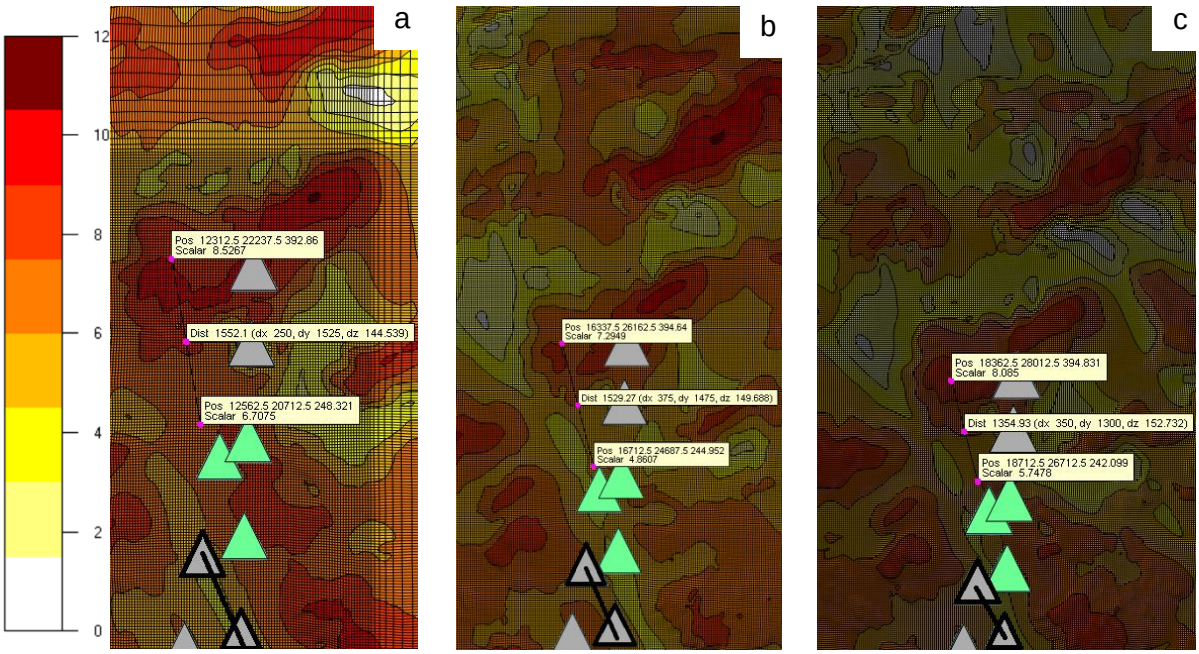

Figure 35 2D wind speed graphics incl. horizontal grid for S1(a), S16(b) and S17(c). Green turbines T25, T2 and T24 (North to South). Black outlined turbines T3 (Top) and T23 (Bottom). Scalar value is the simulated wind speed at the height above terrain H=100

5.4 Vertical Distribution

The results for the vertical distribution shows tendencies in the same direction as the results for resolution and refinement, with a gradual distribution between the cases with the highest and lowest number of cells. From the bar-charts it can be seen that the vertical parameter is not as sensitive as the horizontal resolution parameter. Comparing turbines *T16, T23* and *T26* which have the greatest variety in simulated wind speed shows the same pattern for both numerical settings. It could be argued that even though the variation in wind speed is not significant for all turbines, a higher cell density is desired to get accurate results for the whole wind farm. Inaccurate predictions just for a few turbines can have a great impact on the wind farms total production. The difference between the vertical cases consists through the z-direction. In Figure 38 the distribution of the first 20 cells in the z-direction for cases *S1, S18, S19* and *S20* is displayed. Case *S18* covers the first 100 meters above ground with 5 layers, while case *S20* has 18 layers in the same interval. Since the results are gradually changing with increased number of cells it can be assumed that more cells predict more accurate results. Figure 36 shows the vertical plots for the vertical distribution cases at *M1*, located on the Nevlandsheia hill. The blue line of the *S18* case overestimates the wind speed compared to the other three cases. The wind profiles are gradually distributed with the increase in vertical resolution. At turbine *T23*, located in a

valley, the vertical plot of the *S18* case deviates from the other three cases (Figure 37). There seem to be an underprediction of the windspeed close to the ground and an overprediction when the height above ground surpasses 100m. Again, the other three cases are gradually distributed, but this time towards higher wind speed with higher vertical resolution.

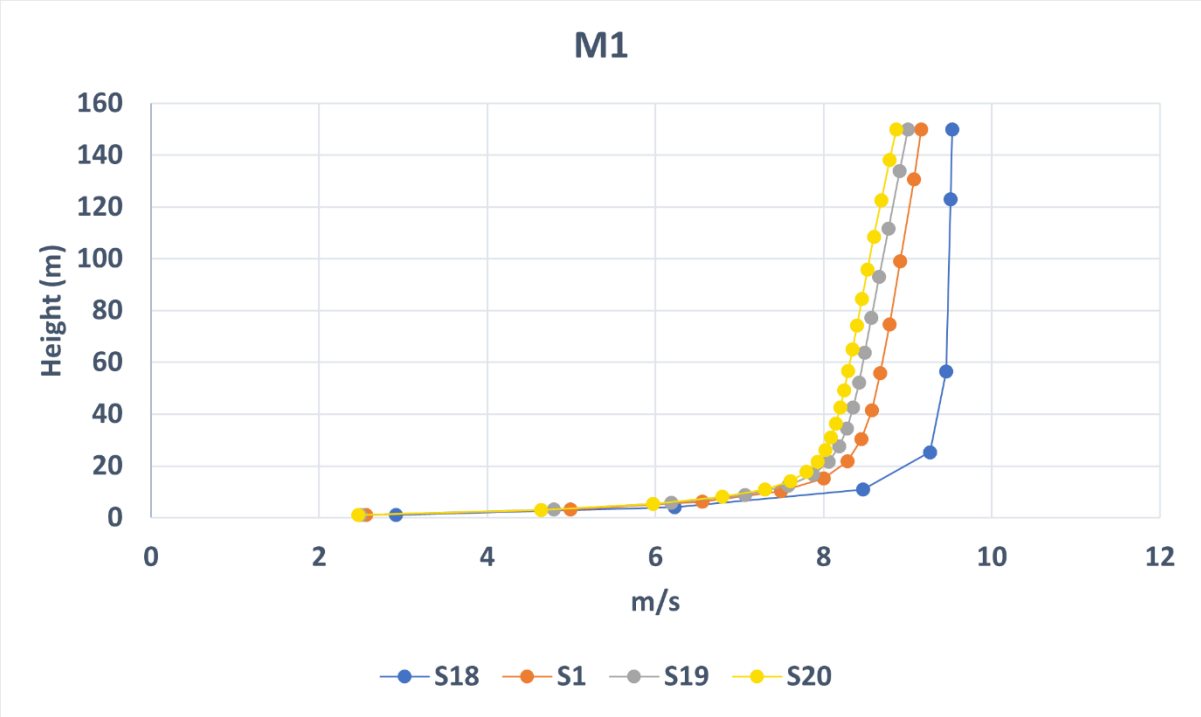

Figure 36 Vertical plot of the simulated wind speed at respective heights at turbine position M1

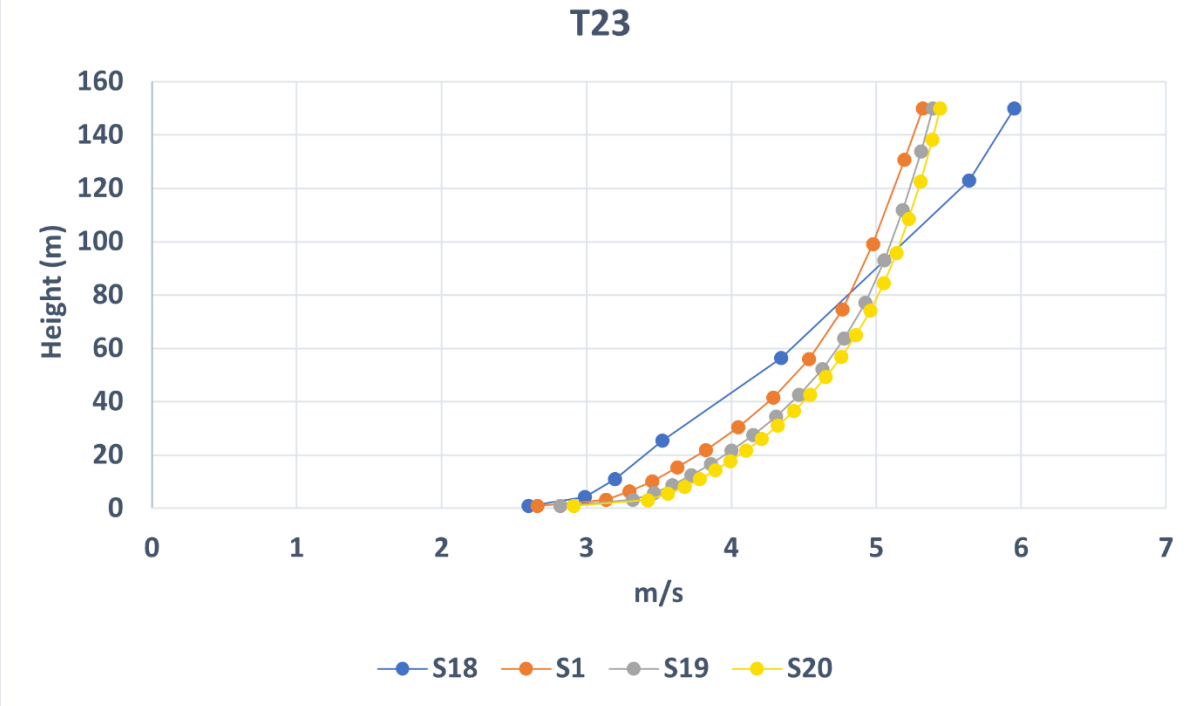

Figure 37 Vertical plot of the simulated wind speed at respective heights at turbine position T23

a

.	1	2	3	4	5	6	7	8	9	10
z-dist. max (m)	1.0	4.1	10.9	25.4	56.4	123.0	265.8	572.1	1229.1	2638.6
z-dist. min (m)	1.0	4.2	10.9	25.4	56.4	123.0	265.8	572.1	1229.2	3027.7

b

.	1	2	3	4	5	6	7	8	9	10
z-dist. max (m)	1.0	3.3	6.3	10.2	15.2	21.8	30.4	41.5	55.8	74.6
z-dist. min (m)	1.0	3.3	6.3	10.2	15.2	21.8	30.4	41.5	55.8	74.6

.	11	12	13	14	15	16	17	18	19	20
z-dist. max (m)	99.0	130.8	172.0	225.5	295.2	385.7	503.4	656.5	855.4	1114.1
z-dist. min (m)	99.0	130.8	172.0	225.6	295.2	385.8	503.5	656.5	855.5	1114.1

c

.	1	2	3	4	5	6	7	8	9	10
z-dist. max (m)	1.0	3.2	5.8	8.7	12.3	16.6	21.6	27.5	34.5	42.6
z-dist. min (m)	1.0	3.2	5.8	8.8	12.4	16.6	21.6	27.5	34.5	42.6

.	11	12	13	14	15	16	17	18	19	20
z-dist. max (m)	52.2	63.7	77.1	93.0	111.7	133.9	160.0	190.8	227.1	270.0
z-dist. min (m)	52.2	63.7	77.2	93.0	111.8	133.9	160.0	190.8	227.1	270.0

d

.	1	2	3	4	5	6	7	8	9	10
z-dist. max (m)	1.0	3.1	5.5	8.0	10.9	14.2	17.8	21.7	26.1	31.0
z-dist. min (m)	1.0	3.1	5.4	8.0	10.9	14.2	17.8	21.7	26.1	31.0

.	11	12	13	14	15	16	17	18	19	20
z-dist. max (m)	36.5	42.5	49.2	56.7	65.0	74.2	84.5	95.8	108.5	122.5
z-dist. min (m)	36.4	42.5	49.2	56.7	65.0	74.2	84.4	95.8	108.4	122.5

Figure 38 The distribution of the first 20 layers in the vertical for cases S18 (a), S1 (b), S19 (c) and S20 (d).

6. Conclusion

The sensitivity of the input parameters defining the numerical grid for wind simulations in complex terrain has been analysed and discussed. The grid resolution is the parameter most sensitive to changes, showing large variations in simulated wind speed, especially at positions close to hills and ridges. Wind turbines are regularly placed in complex terrain to utilize the wind speed-up, but such topography produces regions of high shear and turbulence. Identifying areas of low wind speed and potential recirculation zones requires a high-resolution model.

With respect to the size of the model the results indicate that having a sufficiently large buffer zone around the area of interest in the centre is crucial. The combination of complex terrain and a small domain might cause artificial speed-ups close to the border and the results should be treated with care.

The numerical setting of the refinement area, the area with the maximum cell resolution in the centre of the model, shows a gradually change in result as the number of cells is increased. The same goes for the number of layers in the vertical direction.

There seem to be a quite strong correlation between number of cells and simulated wind speeds. It can be assumed that by increasing the number of cells by changing one of the parameters in the study, the results will become more accurate. The sensitivity of the parameter indicates what numerical setting should be prioritized when creating a wind simulation model. In a step-by-step procedure the most sensitive parameter should be optimized and from the results of this study the maximum resolution of the grid and a sufficient domain size should be prioritized.

The rapid increase in computational power and the introduction of cloud computation enables users to run bigger models more efficiently. In the years to come large models with large number of cells might no longer be a challenge in the field of CFD simulations.

7. Future Improvements/Further Research

Future research should consider:

- Replicating the study for other sites to check if the presented results are reproduced
- Utilize smoothing and the nesting technique as alternatives to increasing the simulation domain.
- In the current study two measurement points are used to validate, having additional points as reference would be useful.
- Including a grid with resolution finer than 10m.
- Run simulations for more than one wind direction
- Analyse how the development of a recirculation on the lee side of a Cosine-hill potentially could affect the speed-up over the hill.

The points above could identify some of the shortcomings of the present study in regards of grid dependency and validation of the results.

References

Abdi, D.S. and Bitsuamlak, G.T. (2014). Wind flow simulations on idealized and real complex terrain using various turbulence models. *Advances in Engineering Software*, 75, pp.30–41.

AIAA (1998). Guide for the verification and validation of computational fluid dynamics simulations. Reston, Va, USA, American Institute of Aeronautics and Astronautics.

Berge, E., Gravdahl, A. R., Schelling, J., Tallhaug, L., Undheim, O. (2006). Wind in complex terrain. A comparison of WAsP and two CFD-models. *Proceedings EWEC*, Athens, Greece.

Blue Marble Geographics. (n.d.). *Global Mapper*. [online] Available at: https://www.bluemarblegeo.com/global-mapper/ [Accessed 26 Nov. 2021].

Carpenter, P. and Locke, N. (1999). Investigation of wind speeds over multiple two-dimensional hills. *Journal of Wind Engineering and Industrial Aerodynamics*, 83(1-3), pp.109–120.

Castro, F. A., Palma, J.M.L.M., Silva Lopes, A. (2003). 'Simulation of the Askervein flow. Part 1: Reynolds averaged Navier-Stokes equations (k-e Turbulence model)' Boundary Layer Meteorology. Vol 107, pp. 501-530.

Cattin, R., Schaffner, B., and Dr. Kunz, S. (2006). Validation of CFD Wind Resource Modeling in Highly Complex Terrain.

Copernicus.eu. (2018). *CLC 2018 — Copernicus Land Monitoring Service*. [online] Available at: https://land.copernicus.eu/pan-european/corine-land-cover/clc2018.

Dhunny, A.Z., Lollchund, M.R. and Rughooputh, S.D.D.V. (2017). Wind energy evaluation for a highly complex terrain using Computational Fluid Dynamics (CFD). *Renewable Energy*, 101, pp.1–9.

Dhunny, A.Z., Lollchund, M.R. and Rughooputh, S.D.D.V. (2016). Numerical analysis of wind flow patterns over complex hilly terrains: comparison between two commonly used CFD software. *International Journal of Global Energy Issues*, 39(3/4), p.181.

Google (2021). *Google Earth*. [online] Google.com. Available at: https://earth.google.com/web/.

Hoydedata.no. (n.d.). *Høydedata*. [online] Available at: https://hoydedata.no/LaserInnsyn/.

Llombart, A., Talayero, A., Mallet, A., Pera, A. and Telmo, E. (2006). Performance analysis of wind resource assessment programs in complex terrain. *Renewable Energy and Power Quality Journal*, 1(04), pp.301–306.

Miller, C.A. and Davenport, A.G. (1998). Guidelines for the calculation of wind speed-ups in complex terrain. *Journal of Wind Engineering and Industrial Aerodynamics*, 74-76, pp.189–197.

Montavon, C., Jones, I., Staples, C., Strachan, C. and Gutierrez, I. (2009) Practical Issues In The Use Of Cfd For Modelling Wind Farms. European Wind Energy Conference.

Palma, J.M.L.M., Castro, F.A., Ribeiro, L.F., Rodrigues, A.H. and Pinto, A.P. (2008). Linear and nonlinear models in wind resource assessment and wind turbine micro-siting in complex terrain. *Journal of Wind Engineering and Industrial Aerodynamics*, 96(12), pp.2308–2326.

Ramechecandane, S. and Gravdahl, A.R. (2012). Numerical Investigations on Wind Flow over Complex Terrain. *Wind Engineering*, 36(3), pp.273–295.

Ramos, D., Guedes, V., Pereira, R., Valentim, T. and Netto, W. (2017). *Further considerations on WAsP, OpenWind and WindSim comparison study: Atmospheric flow modelling over complex terrain and energy production estimate*. [online] Available at: http://viegd.com.br/wp-content/uploads/2017/08/BWP_2017_DANIEL_AGNESE_RAMOS_ARTICLE_2.pdf

Stangroom, P. (2004). *CFD modelling of wind flow over terrain*. [online] eprints.nottingham.ac.uk. Available at: http://eprints.nottingham.ac.uk/10112/.

Tabas, D., Fang, J. & Porté-Agel, F. (2019). Wind Energy Prediction in Highly Complex Terrain by Computational Fluid Dynamics. *Energies*, 12(7), p.1311. Available at: http://dx.doi.org/10.3390/en12071311.

Versteeg, H.K. and Weeratunge Malalasekera (2007). *An introduction to computational fluid dynamics: the finite volume method*. Harlow: Pearson Education.

Wallbank, T. (2008). WindSim Validation Study, CFD validation in Complex terrain. Master's Thesis, Victoria University, Melbourne, Australia.

Norges miljø- og biovitenskapelige universitet
Noregs miljø- og biovitskapelege universitet
Norwegian University of Life Sciences

Postboks 5003
NO-1432 Ås
Norway